HHS Public Access

Author manuscript

Sci Transl Med. Author manuscript; available in PMC 2018 September 20.

Published in final edited form as:

Sci Transl Med. 2017 September 20; 9(408): . doi:10.1126/scitranslmed.aah5360.

Neutrophil transfer of *miR-223* to lung epithelial cells dampens acute lung injury in mice

Viola Neudecker[1,2,*], **Kelley S. Brodsky**[1], **Eric T. Clambey**[1], **Eric P. Schmidt**[1,3], **Thomas A. Packard**[4], **Bennett Davenport**[1], **Theodore J. Standiford**[5], **Tingting Weng**[6], **Ashley A. Fletcher**[7], **Lea Barthel**[8], **Joanne C. Masterson**[9], **Glenn T. Furuta**[9], **Chunyan Cai**[10], **Michael R. Blackburn**[6], **Adit A. Ginde**[1,11], **Michael W. Graner**[12], **William J. Janssen**[1,8], **Rachel L. Zemans**[8], **Christopher M. Evans**[1,7], **Ellen L. Burnham**[7], **Dirk Homann**[1], **Marc Moss**[7], **Simone Kreth**[2], **Kai Zacharowski**[13], **Peter M. Henson**[1,4], and **Holger K. Eltzschig**[1,14]

[1]Organ Protection Program, Department of Anesthesiology, University of Colorado Denver, Aurora, CO 80045, USA

[2]Department of Anesthesiology, University Hospital, Ludwig-Maximilian University of Munich, 81377 Munich, Germany

[3]Program in Translational Lung Research, Department of Medicine, University of Colorado School of Medicine, Aurora, CO 80045, USA

[4]Department of Immunology and Microbiology, University of Colorado Denver School of Medicine and National Jewish Health, Denver, CO 80206, USA

[5]Division of Pulmonary and Critical Care Medicine, University of Michigan Medical School, Ann Arbor, Ml 48109, USA

[6]Department of Biochemistry and Molecular Biology, University of Texas–Houston Medical School, Houston, TX 77030, USA

[7]Division of Pulmonary Sciences and Critical Care Medicine, Department of Medicine, University of Colorado School of Medicine, Aurora, CO 80045, USA

[8]Department of Medicine, National Jewish Health, Denver, CO 80206, USA

[*]Corresponding author. viola.neudecker@med.uni-muenchen.de.

Author contributions: V.N. designed and performed all experiments, wrote the paper, and compiled all original data. H.K.E. provided major funding and essential mentoring and the overall research direction, wrote the manuscript, and reviewed all the original data. Major experimental and technical support was provided by K.S.B. (real-time PCR and immunoblotting), E.P.S. (closed-chest pulmonary intravital microscopy), TAP. (isolation of AT-II epithelial cells), B.D. (bone marrow chimeric mouse experiments), T.W. (histology), A.A.F. (bacterial infection model), L.B. (microvesicle detection), J.C.M. and G.T.F. (PARP-1 enzyme activity assay), M.W.G. (microvesicle preparation), WJJ. (microvesicle detection), C.M.E. (bacterial infection model), and R.L.Z. (RAGE and T1α measurements and TUNEL assay). Extensive review of the manuscript and critical contributions to the concept and direction of the research were provided by E.T.C., E.P.S., T.J.S., M.R.B., A.A.G., M.W.G., W.J.J., R.L.Z., C.M.E., E.L.B., D.H., M.M, S.K., K.Z., and P.M.H. K.S.B. reviewed the original data. Extensive review of statistical analysis for all original data was provided by C.C. All authors contributed to the interpretation of the data and approved the final version of the manuscript.

Competing interests: The authors declare that they have no competing interests.

Data and materials availability: Microarray data have been deposited at www.ncbi.nlm.nih.gov/geo/ (accession number GSE47625). Requests for *miR-223*$^{-/y}$ mice should be made to V. Dawson.

SUPPLEMENTARY MATERIALS

www.sciencetranslationalmedicine.org/cgi/content/full/9/408/eaah5360/DC1

[9]Section of Pediatric Gastroenterology, Hepatology and Nutrition, Gastrointestinal Eosinophilic Diseases Program, Department of Pediatrics, Digestive Health Institute, Children's Hospital Colorado; Mucosal Inflammation Program, Department of Medicine, University of Colorado School of Medicine, Aurora, CO 80045, USA

[10]Department of Internal Medicine, McGovern Medical School, University of Texas Health Science Center at Houston, Houston, TX 77030, USA

[11]Department of Emergency Medicine, University of Colorado School of Medicine, Aurora, CO 80045, USA

[12]Department of Neurosurgery, University of Colorado Denver, Aurora, CO 80045, USA

[13]Department of Anesthesiology, Intensive Care Medicine and Pain Therapy, University Hospital Frankfurt, 60590 Frankfurt am Main, Germany

[14]Department of Anesthesiology, McGovern Medical School, University of Texas Health Science Center at Houston, Houston, TX 77030, USA

Abstract

Intercellular transfer of microRNAs can mediate communication between critical effector cells. We hypothesized that transfer of neutrophil-derived microRNAs to pulmonary epithelial cells could alter mucosal gene expression during acute lung injury. Pulmonary-epithelial microRNA profiling during coculture of alveolar epithelial cells with polymorphonuclear neutrophils (PMNs) revealed a selective increase in lung epithelial cell expression of microRNA-223 (*miR-223*). Analysis of PMN-derived supernatants showed activation-dependent release of *miR-223* and subsequent transfer to alveolar epithelial cells during coculture in vitro or after ventilator-induced acute lung injury in mice. Genetic studies indicated that *miR-223* deficiency was associated with severe lung inflammation, whereas pulmonary overexpression of *miR-223* in mice resulted in protection during acute lung injury induced by mechanical ventilation or by infection with *Staphylococcus aureus*. Studies of putative *miR-223* gene targets implicated repression of poly(adenosine diphosphate-ribose) polymerase–1 (PARP-1) in the *miR-223*–dependent attenuation of lung inflammation. Together, these findings suggest that intercellular transfer of *miR-223* from neutrophils to pulmonary epithelial cells may dampen acute lung injury through repression of PARP-1.

INTRODUCTION

Acute lung injury manifests as acute respiratory distress syndrome (ARDS) in patients (1). Its clinical features include acute hypoxemic respiratory failure and bilateral pulmonary infiltrates that are not attributable to left heart failure (1–3). During acute lung injury, inflammatory cells, particularly polymorphonuclear neutrophils (PMNs), come into close contact with lung alveolar epithelial cells.

Many research studies have provided insights into intercellular communications regulating neutrophil activation and pulmonary transmigration during acute lung injury (4). These communications include paracrine cross-talk between neutrophils and lung parenchymal cells. For example, previous studies have shown that PMNs release extracellular nucleotides

(for example, adenosine triphosphate) that are converted into adenosine, which dampens pulmonary epithelial inflammation (5, 6) and improves fluid transport during acute lung injury (7,8). Here, we investigated whether PMNs could participate in intercellular communication with lung alveolar epithelial cells through microvesicle-dependent exchange of microRNAs (miRNAs) (9).

miRNAs constitute a family of short noncoding RNA molecules of 20 to 25 nucleotides in length that regulate gene expression at the post-transcriptional level (10). Bioinformatic predictions indicate that more than 60% of all mammalian genes are potentially regulated by miRNAs (11). Although the investigation of functional miRNA target genes has identified putative regulatory functions for miRNAs (12), little is known about the repression of inflammatory genes by miRNAs during acute lung injury. Here, we investigated whether PMN–epithelial cell crosstalk during acute lung inflammation could include the exchange of miRNAs (12).

RESULTS

miR-223 can be transferred from neutrophils to pulmonary epithelial cells

Previous studies have indicated that neutrophil (PMN)–epithelial cell cross-talk can dampen inflammation (13). On the basis of these findings, we hypothesized that during neutrophil–epithelial cell interactions, genetic information in the form of miRNAs could be transferred from PMNs to pulmonary epithelia. To test this hypothesis, we set up an in vitro coculture system of human primary alveolar epithelial cells (HPAEpiC) with freshly isolated human PMNs, where both cell types were separated by a membrane with a pore size of 0.4 μm, preventing direct cell-cell contact (Fig. 1A). After 6 hours of coincubation, we washed the alveolar epithelial cells, isolated miRNAs, and performed a targeted expression analysis of miRNAs known to be expressed in human PMNs (14). We observed a robust (more than 100-fold) selective increase in human *miR-223* (hsa-*miR-223*) (Fig. 1B). Confirmatory studies demonstrated that this increase occurred in a time-dependent manner in human primary alveolar epithelial cells (HPAEpiC) and in the pulmonary epithelial cell line Calu-3 after coculture with human PMNs (Fig. 1C and fig. S1A). Analysis of baseline amounts of hsa-*miR-223* in pulmonary epithelia displayed very low expression of *miR-223* [cycle threshold (C_t) value, 29.14 ± 0.61; culture medium C_t value, 34.52 ± 1.12], whereas PMNs demonstrated high expression of hsa-*miR-223* (C_t value, 7.95 ± 0.40) (fig. S1B). Also, the expression of hsa-*miR-223* in HPAEpiC was not inducible by various stimuli tested including exposure to *N*-formyl-Met-Leu-Phe (*f*MLP) or lipopolysaccharide (LPS) (Fig. 1, D and E). In contrast, hsa-*miR-223* was found to be about 20-fold lower after coculture of PMNs with human microvascular endothelial cell–1 (HMEC-1) (15, 16) than coculture with human pulmonary epithelial cells (Calu-3) (fig. S1C). To test whether the hsa-*miR-223* detected in human pulmonary epithelial cells after coculture was functional, we performed coculture studies with human pulmonary epithelial cells (Calu-3) that were previously transfected with a luciferase reporter carrying a *miR-223* target sequence. Significant decreases ($P < 0.05$) in luciferase activity in Calu-3 after coculture indicated that hsa-*miR-223* was functional after coculture (Fig. 1F). To provide additional evidence that increases in pulmonary epithelial cell *miR-223* after coculture were due to PMNs, we used a

murine coculture system that allowed us to study *miR-223*-deficient PMNs (Fig. 1G). In this system, a murine pulmonary epithelial cell line (MLE-12) was cocultured with murine PMNs derived from either wild-type or *miR-223*$^{-/y}$ mice. The *miR-223* gene is located on the X chromosome; therefore, the knockout mice were hemizygous for *miR-223* (*miR-223*$^{-/y}$). The deficiency in *miR-223* was confirmed by analyzing *miR-223* in murine neutrophils from *miR-223*$^{-/y}$ mice compared to wild-type mouse neutrophils (fig. S1, D and E). Analyses of murine *miR-223* (mmu-*miR-223*) after 6 hours of coculture with wild-type PMNs revealed a significant increase ($P < 0.05$), whereas no alteration in epithelial cell mmu-*miR-223* expression was observed after coculture with murine PMNs derived from *miR-223*$^{-/y}$ mice (Fig. 1H). Moreover, a comparison of *miR-223* shuttling in the coculture system comprising murine alveolar epithelial cell type I or II (AT-II–like cells, MLE-12 cell line; AT-I–like cells, E-10 cell line; Fig. 1I) indicated that *miR-223* transfer predominantly occurred from neutrophils to AT-II cells. Together, these findings indicate that *miR-223* can be transferred from PMNs to pulmonary epithelial cells under coculture conditions.

miR-223 release from PMNs is activation-dependent

Next, we examined the supernatant from PMNs for *miR-223* content. PMNs released high amounts of *miR-223* into the supernatant (Fig. 2A). Isolation of microvesicles from the supernatant from PMNs via ultracentrifugation showed a high concentration of *miR-223* (Fig. 2B). In addition, incubation of PMN supernatants with HPAEpiC was associated with increased *miR-223* in HPAEpiC, whereas this response was almost completely abolished when using PMN supernatants that lacked the microvesicle fraction (Fig. 2C). Besides the secretion of microvesicles, activation of PMNs induced the release of decondensed chromatin and granular contents into the extracellular space (17). These structures, called neutrophil extracellular traps (NETs), have antimicrobial properties but have also been implicated in inflammation. We therefore asked whether the release of NETs (NETosis) was involved in the secretion of *miR-223* by PMNs. As shown previously, we observed that activation of PMNs was associated with increased NETosis (fig. S2A). To address the possibility that increased NETosis could also be associated with increased release of *miR-223*, we repeated these studies in the presence of a NETosis inhibitor. Effective inhibition of NETosis did not affect *miR-223* release, thereby providing evidence that NETosis was not a major pathway mediating extracellular *miR-223* release (fig. S2, A and B). To provide further evidence for PMN-epithelial cell miRNA transfer, we transfected a human neutrophil–like cell line (HL-60) with cel-*miR-39*, a miRNA only present in *Caenorhabditis elegans*, and assessed cel-*miR-39* expression in human pulmonary epithelial cells (Calu-3) after coculture. We found a robust increase in cel-*miR-39* in human pulmonary epithelial cells (Calu-3) (fig. S2C). Moreover, the addition of monodansylcadaverine (a known inhibitor of clathrin-mediated endocytosis) to the supernatant partially attenuated the alveolar epithelial cell uptake of *miR-223*-containing microvesicles, thus implicating clathrin-mediated endocytosis in *miR-223* transfer (Fig. 2D). Consistent with our work showing PMN transfer of *miR-223* into AT-II cells (Fig. 1I), previous studies have demonstrated that clathrin-mediated transport is functionally important in AT-II cells (18, 19). Together, these findings suggest that *miR-223*-containing microvesicles may be released from PMNs after PMN activation and then could be transferred into alveolar epithelial cells.

PMNs are required for increased pulmonary *miR-223* during acute lung inflammation

Given that neutrophils are in close contact with pulmonary epithelial cells during lung inflammation, we next examined mmu-*miR-223* expression during acute lung inflammation in mice. For this purpose, we used a mouse model where lung injury was induced by mechanical ventilation [ventilator-induced lung injury (VILI)] (7, 20–22). We found that mmu-*miR-223* in whole lungs was significantly increased after induction of acute lung inflammation in mice ($P < 0.05$; Fig. 2E). This increase was associated with an increase in PMN-derived ($CD11b^+Ly6G^+$) microvesicles (fig. S3, A and B). In line with a possible transfer of *miR-223* from PMNs to alveolar epithelial cells during acute lung inflammation, we found that mmu-*miR-223* in isolated mouse alveolar epithelial cells was elevated after induction of acute lung inflammation (Fig. 2F), whereas *miR-223* expression in isolated mouse pulmonary endothelial cells remained the same (fig. S3C). To generate mice chimeric for *miR-223*, wild-type mice underwent sublethal radiation and were transplanted with *miR-223*$^{-/y}$ mouse bone marrow and vice versa. Studies of these bone marrow chimeric mice revealed that increased mmu-*miR-223* in mouse alveolar epithelial cells during pulmonary inflammation was predominantly dependent on the presence of mmu-*miR-223* in bone marrow–derived cells (Fig. 2G and fig. S4, A to C). Similarly, increased mmu-*miR-223* expression during acute lung inflammation was attenuated after antibody depletion of PMNs (Fig. 2H and fig. S4, D and E). Although the antibody treatment resulted in significant neutrophil depletion, it did not affect monocytes (fig. S4E). Consistent with these findings, *miR-223* expression was more than 25-fold higher in PMNs than in alveolar macrophages (AM ϕ) (fig. S5A), and transfer of *miR-223* from bone marrow–derived macrophages (BMDM ϕ) to mouse pulmonary epithelial cells was not detectable during coculture (fig. S5B). Moreover, induction of *miR-223* expression during acute lung inflammation induced by mechanical ventilation remained intact after macrophage depletion with clodronate (fig. S5C). To study PMN-dependent miRNA release during acute lung injury in mice, we examined animals that had been injected with PMN-like cells (HL-60) that had been transfected with a synthetic fluorescently labeled miRNA. Intravital microscopy through a transthoracic window revealed evidence for release of miRNAs from HL-60 cells that were in close proximity to mouse alveolar epithelial cells during acute lung injury induced by mechanical ventilation (Fig. 2I). In addition, costaining for AT-II cells (Fig. 2J, green) in murine lung tissue sections from ventilated mice that had been injected with labeled PMN-like cells (HL-60; Fig. 2J, red) suggested that there may also have been transfer of cytoplasm from the PMN-like cells in vivo. Moreover, we also observed that patients with ARDS (Table 1) showed increased hsa-*miR-223* in their bronchoalveolar lavage (BAL) fluid compared to healthy control patients (control group mean C_t value for *miR-223*, 26.61; mean C_t value for control ce–*miR-39*, 23.32; ARDS group mean C_t value for *miR-223*, 25.35; mean C_t value for control ce–*miR-39*, 24.23) (Fig. 2K). Together, these findings indicate that PMN-dependent production of mmu-*miR-223* contributed to increased *miR-223* expression in injured mouse lungs after mechanical ventilation and suggest that *miR-223* was transferred to mouse alveolar epithelial cells during acute lung inflammation.

PARP-1 is a *miR-223* target gene in pulmonary epithelial cells

We next performed studies to identify *miR-223* target genes in pulmonary epithelial cells. For this purpose, we used lentiviral transduction to generate a pulmonary epithelial cell line

(Calu-3) that overexpressed *miR-223* (Fig. 3, A and B). A whole-genome microarray comparing control- transfected Calu-3 cells with Calu-3 *miR-223*-overexpressing cells identified 83 genes with decreased expression in the *miR-223*-overexpressing cell line (table S1). Among genes containing a *miR-223* seed match (TargetScan, miRanda, MicroCosm, and miRDB), the gene most robustly repressed after *miR-223* overexpression was poly[adenosine diphosphate (ADP)–ribose] polymerase–1 (PARP-1). PARP-1 is known to facilitate inflammatory responses by activating transcription factors such as nuclear factor κB (NF-κB) and activator protein–1 (AP-1). PARP-1 drives inflammation-relevant gene expression via various proinflammatory cytokines, adhesion molecules, and enzymes involved in inflammation. Previous studies demonstrated a detrimental role for PARP-1 during acute lung injury induced by mechanical ventilation (23). In line with studies from the cancer field (24), we confirmed repression of PARP-1 transcripts (Fig. 3C) and protein (Fig. 3, D and E) after *miR-223* overexpression. We next utilized two luciferase reporter plasmids with one containing the wild-type 3′ untranslated region (3′UTR) of PARP-1 and the other carrying a mutated version where specific binding of *miR-223* to the 3′UTR was abrogated (Fig. 3F). Transfection of these plasmids into human pulmonary epithelial cells confirmed repression of the wild-type PARP-1 plasmid after *miR-223* overexpression, which did not occur with the mutated plasmid (Fig. 3, G and H). A coculture system comprising human PMNs and human pulmonary epithelial cells (Calu-3) (Fig. 1A) revealed repression of PARP-1 transcripts in the pulmonary epithelial cells (Fig. 3I). Together, these findings identify PARP-1 as a *miR-223* target gene.

miR-223$^{-/y}$ mice develop severe lung inflammation during acute lung injury

To address the functional role of *miR-223* during pulmonary inflammation, we next performed genetic studies in *miR-223*$^{-/y}$ mice (25). We induced acute lung injury using mechanical ventilation in *miR-223*$^{-/y}$ mice or wild-type control mice matched for age, gender, and weight Consistent with a functional role for *miR-223* in repressing inflammatory gene expression, we found that, compared to control mice, *miR-223*$^{-/y}$ mice showed increased permeability of lung alveolar cells (Fig. 4A). The *miR-223*$^{-/y}$ mice also showed greater lung inflammation as assessed by measurement of bronchoalveolar myeloperoxidase (Fig. 4B), bronchoalveolar cytokines (Fig. 4, C and D), histological tissue injury (Fig. 4, E and F), and lung wet- to-dry weight ratios (fig. S6A). The repression of PARP-1 protein during VILI seen in wild-type mice was attenuated in *miR-223*-deficient mice (Fig. 4, G and H). In addition, analysis of PARP-1 enzyme activity revealed increased PARP-1 activity in *miR-223*$^{-/y}$ animals (Fig. 4, I and J). Moreover, *miR-223*-deficient mice also experienced increased tissue inflammation during pulmonary infection with methicillin-resistant *Staphylococcus aureus* (strain USA300). At early time points (4 hours after infection), *miR-223*$^{-/y}$ mice showed increased permeability of alveoli to proteins, elevated myeloperoxidase in the BAL, and augmented inflammatory cytokine production in pulmonary tissue (Fig. 5, A to G). In addition, mice lacking mmu-*miR-223* showed significantly reduced survival during acute lung inflammation induced by *S. aureus* infection compared to wild-type mice ($P < 0.05$; Fig. 5H). Analysis of bacterial clearance revealed no significant difference between wild-type and *miR-223*$^{-/y}$ mice (Fig. 5, I and J), indicating that reduced survival in mice lacking mmu-*miR-223* was unlikely to be due to reduced bacterial killing.

To demonstrate that increased lung inflammation and more severe acute lung injury in *miR-223*$^{-/y}$ mice were related to the *miR-223* target gene PARP-1, we attempted to reverse the phenotype of *miR-223*$^{-/y}$ mice by repressing PARP-1 genetically using lentiviral transduction with a short hairpin RNA (shRNA) vector that was specific for PARP-1. Intratracheal administration of lentiviral shRNA was associated with reduced PARP-1 protein and PARP-1 enzyme activity at baseline and after VILI (Fig. 6, A to D). Functional studies analyzing the outcome after induction of VILI demonstrated that lentiviral shRNA-mediated PARP-1 repression in *miR-223*$^{-/y}$ mice was associated with a reversal of the lung inflammation phenotype (Fig. 6, E to K). Measurements of the alveolar epithelial injury markers RAGE (receptor for advanced glycation end-products) and the alveolar cell protein T1α revealed lower concentrations of both molecules in *miR-223*$^{-/y}$ mice with shRNA-mediated PARP-1 repression (fig. S7, A and B). In addition, these mice also showed lower numbers of TUNEL (terminal deoxynucleotidyl transferase-mediated deoxyuridine triphosphate nick end labeling)-positive cells, implying a reduced cell death rate after PARP-1 repression (fig. S7C).

Collectively, these studies demonstrate that genetic deletion of *miR-223* promoted increased lung injury during acute pulmonary inflammation induced by mechanical ventilation or bacterial infection. In addition, pulmonary edema and lung inflammation in *miR-223*$^{-/y}$ mice were reduced by overexpression of mmu-miR-223 and repression of PARP-1.

Inducing pulmonary *miR-223* overexpression with nanoparticles dampens acute lung inflammation

We next pursued the possibility that overexpression of *miR-223* was associated with lung protection during acute lung injury induced by mechanical ventilation. For this purpose, we treated wild-type mice endotracheally with nanoparticles containing synthetic *miR-223* mimics (26). This treatment was associated with robust repression of PARP- 1 transcripts in mouse alveolar epithelial cells (Fig. 7A). Previous studies using a PARP-1 inhibitor (PJ34) revealed that PARP-1 repression was beneficial during pulmonary inflammation, suggesting that *miR-223*-elicited PARP-1 repression could be useful for treating acute lung injury (23). Functional studies of lung inflammation induced by mechanical ventilation demonstrated that pulmonary overexpression of *miR-223* in mouse lungs was associated with decreased albumin detection in the BAL fluid (Fig. 7B) and attenuated lung wet-to-dry weight ratios, indicating improved alveolar-capillary barrier function (Fig. 7C). Pulmonary overexpression of *miR-223* was also associated with attenuated lung inflammation (Fig. 7, D to J). To address the effects of *miR-223* overexpression in an infectious disease model of acute lung injury, we exposed mice intratracheally to methicillin-resistant *S. aureus* (strain USA300). Pulmonary overexpression of *miR-223* attenuated lung edema, inflammation, and tissue injury during pulmonary infection with *S. aureus* (Fig. 8, A to G). Moreover, pulmonary *miR-223* overexpression provided significantly improved mouse survival during acute lung inflammation induced by pulmonary *S. aureus* infection compared to mice treated with a control vector ($P < 0.05$, Mantel-Cox test; Fig. 8H). Analysis of pulmonary bacterial clearance revealed no difference between *miR-223*-overexpressing mice and control animals (Fig. 8, I and J). Pulmonary overexpression of *miR-223* was associated with reduced PARP-1 protein expression (fig. S8, A and B) and a reduction in epithelial cell injury as

measured by lowered T1α protein and reduced cell death (analyzed by TUNEL staining) (fig. S8, C and D).

Together, these data provide evidence that overexpression of *miR-223* was associated with protection from lung inflammation and pulmonary edema during acute lung injury induced by mechanical ventilation or pulmonary *S. aureus* infection.

DISCUSSION

Here, we pursued the hypothesis that during acute lung injury, miRNAs are shuttled from PMNs to pulmonary epithelial cells, thereby providing a feedback mechanism to dampen inflammatory gene expression and lung inflammation. An experiment where human PMNs were coincubated with HPAEpiC revealed a selective increase in *miR-223* expression by alveolar lung epithelial cells. Basal expression of *miR-223* in HPAEpiC was very low, and external stimulation with LPS or fMLP failed to induce endogenous up-regulation of *miR-223*. Genetic studies using a coculture system comprising PMNs derived from *miR-223*$^{-/y}$ mice demonstrated that this increase in *miR-223* reflected transfer of *miR-223* from PMNs to the pulmonary epithelial cells. Moreover, further studies demonstrated that the release of *miR-223* into the supernatant was increased upon activation of the PMNs and that transfer of *miR-223* into alveolar epithelial cells was mediated by microvesicles. Studies of *miR-223* target genes in human pulmonary epithelial cells indicated that anti-inflammatory functions of *miR-223* during acute lung injury involved the *miR-223* target gene PARP-1. Functional studies demonstrated that *miR-223*$^{-/y}$ mice were prone to acute lung inflammation induced by mechanical ventilation and that endotracheal application of *miR-223*-containing nanoparticles reversed this phenotype. Treatment with *miR-223*-containing nanoparticles provided protection from lung inflammation and pulmonary edema in wild-type mice during acute lung injury induced by mechanical ventilation or pulmonary infection with *S. aureus*. Together, these findings implicate PMN-dependent *miR-223* transfer in an endogenous feedback mechanism that may limit excessive lung inflammation during acute lung injury via repression of PARP-1 (Figs. 7 and 8).

Previous studies have implicated *miR-223* in PMN development and function. Human granulocytic differentiation is controlled by a regulatory circuitry involving *miR-223*, indicating that *miR-223* may play a crucial role during granulopoiesis (27, 28). Other studies suggest that *miR-223* expression might be driven by myeloid transcription factors (29). Meanwhile, studies using a loss-of-function allele in mice show that *miR-223* negatively regulates myeloid progenitor cell proliferation and granulocyte differentiation and activation. In those initial studies, stimulation of mouse wild-type and *miR-223*$^{-/y}$ neutrophils with different concentrations of phorbol 12-myristate 13-acetate (PMA) led to production of lower amounts of reactive oxygen metabolites. Additionally, the observed percentage of wild-type versus *miR-223*$^{-/y}$ PMNs that underwent a respiratory burst was much lower. On the basis of those initial studies generating and characterizing the *miR-223*$^{-/y}$ mouse phenotype, the lack of *miR-223* in the mutant mouse neutrophils induced a hypersensitive state in response to activating stimuli (25). As a consequence of this neutrophil hyperactivity, *miR-223*$^{-/y}$ mice spontaneously develop inflammatory lung pathology and exhibit exaggerated tissue destruction after endotoxin challenge (25). Our study indicates

that *miR-223* dampens lung injury induced by mechanical ventilation or by pulmonary infection with *S. aureus*.

We identified PARP-1 as a target gene of *miR-223* in pulmonary epithelia. PARP-1 is a member of the PARP family, which is composed of enzymes that catalyze a posttranslational modification called poly (ADP-ribosyl)ation (30). PARP-1 is expressed in all mammalian cells except mature granulocytes, which is in line with our findings that *miR-223*-dependent lung protection involves the transfer of *miR-223* to another cell type. PARP-1 is involved in the regulation of various biological activities, including DNA repair, DNA replication, transcription, and proteasomal degradation. However, PARP-1 has also been implicated in inflammation and in ischemia-reperfusion tissue injury (30–32). Consequently, pharmacological inhibition or genetic deletion of PARP-1 has been shown to protect against inflammatory diseases, such as acute lung injury. Our findings of *miR-223*-dependent PARP-1 repression during acute lung injury are in line with an anti-inflammatory role for *miR-223* shuttled by PMNs during pulmonary inflammation (31). Our observations in *miR-223*$^{-/y}$ mice using PARP-1 shRNA to inhibit PARP-1 expression during pulmonary inflammation are consistent with previous studies where PARP-1 inhibitors decreased lung permeability in lung injury mouse models (31). The improved barrier function we observed during induction of lung inflammation by mechanical ventilation in *miR-223*$^{-/y}$ mice with shRNA-mediated PARP-1 inhibition, indicated by reduced albumin leakage and diminished lung edema, is in agreement with observations in other inflammatory diseases. For example, pharmacological PARP-1 inhibition resulted in a reduction in proinflammatory cytokine production and in intestinal permeability in a murine model of experimental colitis (33). Similarly, our observations of diminished lung epithelial cell inflammation after transfer of *miR-223* from neutrophils to alveolar epithelial cells indicate an anti-inflammatory and protective role for *miR-223*-mediated PARP-1 inhibition during acute lung injury.

Studies from the cancer field indicate that miRNAs can be released from microvesicles produced by cancer cells and implicate miRNA transfer in tumor expansion and metastasis. Our study suggests that inflammatory cells, such as PMNs, may release miRNAs in microvesicles to provide anti-inflammatory signals to pulmonary epithelial cells. Previous studies have shown that neutrophils can release anti-inflammatory microvesicles upon activation (34, 35). Lung infiltration by activated PMNs has been implicated as a key event in the development of lung inflammation during acute lung injury. The release of *miR-223*–containing microvesicles by PMNs may be a signal for the resolution of epithelial inflammation. Our findings suggest that neutrophils, often thought to only accelerate inflammation and injury, may play a critical role in injury repair potentially by transferring *miR-223* to lung alveolar epithelial cells. These findings are consistent with previous studies implicating neutrophils in epithelial repair of the injured lung (36). Although they are crucial for fighting infection, neutrophils could also contribute to lung injury through several mechanisms that cause collateral damage (37). For VILI, neutrophil infiltration is a key event (38). High-pressure ventilation-induced pulmonary inflammation results in damage to the alveolar-capillary barrier, as shown in our study by increased albumin in the BAL fluid. During VILI, there is an increase in myeloperoxidase produced by neutrophils, indicating a PMN influx into the lungs. Exaggerated neutrophil activation and the release of microbicidal compounds and proinflammatory cytokines into the extracellular space can damage host

tissues. Several studies have shown that depletion of granulocytes during lung injury attenuates inflammation and reduces the severity of lung injury (39, 40). In contrast, in other inflammatory disease models, there is also evidence that neutrophil depletion can aggravate inflammatory disease progression (41). Our study suggests that the infiltrating neutrophils provide an additional protective mechanism through transfer of *miR-223* to the lung epithelium.

The phenomenon of neutrophil-epithelial cross-talk highlighted here was found to occur in different types of pulmonary epithelial cells. This is in line with previous observations that PMNs can migrate across connective tissue and epithelial barriers throughout the respiratory tract. We found some indication that *miR-223* transfer primarily involves AT-II cells of the lung alveoli. AT-II cells have been described as relatively resistant to cell death during acute tissue injury, and *miR-223*-mediated AT-II cell protection may play a functional role during the acute phase of lung injury and repair.

Although our data suggest a functional role for *miR-223*–dependent miRNA transfer during acute lung injury, there are a number of major limitations to our study. Although we observed a protective role for *miR-223* in the acute phase of lung injury and lung infection, the functional role of *miR-223* during chronic states of lung disease and the impact on lung injury resolution remain unknown. Much of our study was carried out in *miR-223*$^{-/y}$ mice with global deletion of *miR-223;* additional studies in mice with *miR-223* deletion in different lung tissue compartments may have the potential to identify additional *miR-223* functions and other target genes. We identified PARP-1 as an epithelial *miR-223* target gene mediating the protective role of *miR-223* during acute lung injury. Given that miRNAs usually regulate multiple target genes, it is likely that there are *miR-223* gene targets in addition to PARP-1 that could be involved in protection against pulmonary inflammation. We only examined global *miR-223* expression in BAL fluid from patients with ARDS, but future studies will need to examine *miR-223* expression in subgroups of patients suffering from lung injury and at diverse stages of disease.

MATERIALS AND METHODS

Study design

We combined several approaches to investigate miRNA transfer from neutrophils to alveolar epithelial cells during acute lung injury in mice. First, we established a coculture system in vitro using PMNs and pulmonary epithelial cells of human or murine origin to study miRNA transfer. Two different murine models of acute lung injury were used to investigate the transfer of *miR-223* during pulmonary inflammation: a mechanical VILI model and a bacterial infection model of acute murine pneumonia. For histology scoring, the researcher was blinded to the treatment group and sample identity. Numbers of replicates for experiments are specified in the corresponding figure legends. Two different genotypes of mice were used to confirm the critical role of *miR-223:* wild-type and *miR-223*$^{-/y}$ mice. To further explore the relevant myeloid cell type as a source of *miR-223*, bone marrow chimeric mice were generated, and depletion studies were conducted. For *miR-223* target identification, microarray analysis and ludferase assays were used. As proof of principle, *miR-223* was overexpressed using nanopartide-packaged *miR-223* mimics. Analysis of

miR-223 in human samples was performed on BAL fluid collected from 55 patients with ARDS within the first 7 days after diagnosis. Demographic and clinical data such as APACHE II scores and primary etiology are shown in Table 1. BAL fluid samples derived from healthy individuals served as controls. All eight control subjects were between 18 and 55 years of age, were not taking any medications, and were lifelong nonsmokers. There were five males and three females.

Cell culture and treatments

Primary alveolar epithelial cells (HPAEpiC, ScienCell Research Laboratories), human airway epithelial cells [Calu-3, American Type Culture Collection (ATCC)], murine alveolar epithelial cells (MLE-12, gift from I. Douglas, Pulmonary Sdences and Critical Care Medicine, School of Medicine University of Colorado, USA; E-10, gift from D. C. Thompson, Department of Clinical Pharmacy, School of Pharmacy University of Colorado, USA), and human promyelocytic leukemia cells (HL-60, ATCC) were cultured according to the manufacturer's instructions and in the appropriate media. During coculture, all cell types were incubated in Hanks' buffer.

Coculture experiments

Coculture experiments were set up using Transwell plates with 0.4-μm pore size polycarbonate membrane inserts (Coming) according to the manufacturer's instructions. Depending on the readout, cocultures were carried out in 6-, 12-, or 24-well inserts. Pulmonary epithelial cells (Calu-3, HPAEpiC, MLE-12, and E-10) were seeded and grown to confluence in the lower chamber before coculture. During coculture, appropriate numbers [a ratio of 1:2 for all experiments, except Fig. 1E (ratio, 1:3)] of either freshly isolated human PMNs (activated with *f*MLP), murine isolated PMNs [activated with PMA (0.1 μg/ml)], or neutrophillike HL-60 cells [differentiated 4 days with dimethyl sulfoxide (DMSO)] were added to the upper chamber, and coculture was carried out for 4 to 6 hours. Under control conditions, epithelial cells were treated with *f*MLP (1 mM) or LPS (10 μg/ml) for 6 hours. At the end of each coculture experiment, PMN-containing inserts were removed, and cells in the lower chamber were washed once with 1× phosphate-buffered saline (PBS), followed by an immediate lysis with QIAzol for RNA analysis. In the case of coculture experiments, luciferase-transfected pulmonary epithelial cells were transfected 24 hours before coculture, inserts were removed after 6 hours of coculture, and transfected cells in the lower chamber were further cultured for another 48 hours before lysis and ludferase activity measurements. In studies analyzing the epithelial microveside uptake mechanism, human pulmonary alveolar epithelial cells (HPAEpiC) were pretreated with 50 μM monodansylcadaverine (MDC; Sigma-Aldrich), an inhibitor of dathrin-dependent endocytosis (42), 30 min before coculture.

Generation of overexpressing miR-223 cell line

Green fluorescent protein (GFP)-miR-223 precursor construct, built in a lentiviral vector backbone (purchased from SBI), was produced by cotransfecting the plasmid with pPACK packaging mix (SBI into 293T cells, ATCC) to generate lentiviral partides. Virus-containing supernatants were harvested according to the manufacturer's instructions (SBI), and Calu-3

were transduced with either GFP-miR-223 lentivirus or GFP-control lentivirus according to the manufacturer's instructions.

Binding of miR-223 to miR-223 target vector or 3′UTR of PARP-1

Cells (Calu-3 or lentiviral-transduced Calu-lenti-223 or Calu-lenti-ctr) were transfeded with PARP-1 3′UTR reporter construct (ludferase vedor containing the 3′UTR of PARP-1 downstream the ludferase gene; OriGene) or miR-223 target vedor (vedor containing a target sequence for miR-223 downstream the ludferase gene; SwitchGear) or with respective control vedors. Forty-eight hours later, cells were harvested, and ludferase activity was measured using the Dual-Luciferase Reporter kit (Promega) (for the PARP-1 3′UTR reporter construd) or the LightSwitch Ludferase Assay Kit (SwitchGear) (for the miR-223 target vedor) according to the manufacturer's instructions.

Isolation of human PMNs

The collection and use of human PMNs from healthy volunteers were approved by the Colorado Multiple Institutional Review Board (COMIRB), and before each blood draw, written informed consent from each individual was obtained. For isolation of human PMNs, human blood was obtained by venipuncture from healthy volunteers. The blood was anticoagulated with an ACD (add-citrate-dextrose) buffer and added to 3% dextran solution for sedimentation. To separate cells, we carefully layered anticoagulated whole blood on top of a density gradient cell separation medium of Ficoll and sodium diatrizoate (Histopaque-1077, Sigma-Aldrich). After centrifugation at 2700 rpm for 30 min at room temperature without break, supernatant was removed, PMNs containing pellet (from this step onward, all steps were carried out at 4°C) were resuspended, and residual erythrocytes were removed with two washes of ice-cold RCLB (red cell lysis buffer) and then washed twice in Hanks' buffer (−). During counting and until experiments were started, PMNs were kept in Hanks' buffer (−) and at 4°C. For activation, PMNs were transferred from Hanks' buffer (−) to Hanks' buffer (+) supplemented with 1 pM/MLP and incubated at 37°C. The viability of the cells after isolation was greater than 97% using the trypan blue dye exclusion test.

Isolation and purification of murine PMNs

Murine PMNs were isolated from the bone marrow of C5BL/6 or *miR-223*$^{-/y}$ mice using the EasySep Mouse Neutrophil Enrichment Kit (STEMCELL Technologies) according to the manufacturer's instructions. The negative selection method was chosen because it is considered to result in less activation (compared to positive selection methods) during the purification procedure. Briefly, mice were euthanized, and the bone marrow was harvested from femurs and tibias. Cells were centrifuged and incubated with a cocktail of biotinylated antibodies for negative selection, again centrifuged and then incubated with EasySep D magnetic particles. Subsequently, cells were placed in an EasySep Magnet to separate and finally decant the nonlabeled purified murine PMNs. All steps were carried out at 4°C to avoid any activation of cells before starting the desired experiment.

Isolation of murine AMϕ

Murine AMϕ were isolated as previously described (43).

Isolation of pulmonary endothelial cells

Murine pulmonary endothelial cells were isolated as previously described (44).

Lung injury score

Murine lung histology was scored blinded according to lung injury scoring criteria published previously (45).

Isolation and culture of murine BMDMϕ

Murine BMDMϕ were isolated and activated as previously described (46).

Microvesicle isolation from PMN supernatant/human BAL samples

PMN-derived microvesicles were isolated by sequential ultracentrifugation as described previously (34). Briefly, after culture of freshly isolated PMNs, supernatants were collected, and cell debris was removed by two consecutive centrifugations (4000*g* for 20 min at 4°C). Then, to collect the PMN-derived microvesides, the supernatants were ultracentrifuged at 160,000g for 60 min at 4°C in a Type 70.1 Ti rotor (Beckman Instruments Inc.). The pelleted microvesicles were further processed depending on the experimental setup; either the pelleted microvesicles were directly lysed in QIAzol for RNA isolation using the RNeasy kit (Qiagen) following the manufacturer's instructions provided or kept in PBS for other experiments.

Microvesicle analysis with flow cytometry

Microvesides were obtained from murine lungs by performing BAL with PBS that had been filtered through a 0.2-μm filter to remove particulate debris. Lavage fluid was then centrifuged at 200*g* for 5 min to pellet cells. One hundred microliters of cell-free supernatant was removed and incubated on ice for 30 min with fluorescently conjugated antibodies directed against CD45 (clone 30-F11, BD Biosciences) and CD11b (clone M1/70, BD Biosdences) at concentrations of 1:100. Control isotype antibodies were added to paired aliquots at similar concentrations. Samples were diluted with 900 μl of filtered PBS and taken to flow cytometry where calibrated fluorescent microveside sizing beads (Megamix, Biocytex) were added at a concentration of 27,000/ml. Microvesides from cultured human neutrophils were analyzed by adding antibodies directed against CD45 (clone TU116, BD Biosdences) and CD11b (clone ICRF44, BD Biosciences) to 100 μl of cell culture supernatant for 30 min. Specimens were diluted in 900 pi of filtered PBS, and Megamix beads were added. Flow cytometry for all experiments was performed on a Gallios 561 cytometer (Beckman Coulter) with a wide-angle forward scatter aperture. Forward and side scatter thresholds were set using calibrated microbeads. Microvesides were enumerated by collecting events between 0.2 and 0.9 μm in size after excluding microbeads based on their fluorescence.

Quantification of NET release from activated neutrophils

NETs were quantified using fluorimetry as described previously (47). Briefly, freshly isolated neutrophils were cultured in 96-well microtiter plates and stimulated with fMLP at a concentration of 1 μM. For inhibition of secretion of NETs, PMNs were pretreated with NETosis inhibitor Cl-Amidine (1 mM for 15 min) (Cayman Chemical). SYTOX Green, a non–cell-permeant DNA binding dye (Thermo Fisher), was added to the cells at 5 μM concentration to detect extracellular DNA. The degree of the fluorescence of treated cells was obtained after subtracting baseline fluorescence of medium only, and the data were normalized as 100% NET formation to the stimulus, leading to the greatest degree of NETosis (stimulation with jMLP) to more readily assess the fold reduction. The plates were read in a fluorescence microplate reader with a filter setting of 485 nm (excitation)/525 nm (emission).

Patient samples

Collection and use of patient samples were approved by the appropriate institutional review board (IRB) of each institution, and COMIRB approval had been obtained. BAL fluid was collected from 55 patients with ARDS within the first 7 days after diagnosis. Demographic and clinical data APACHE II scores and primary etiology are shown in Table 1. BAL fluid samples derived from healthy individuals served as controls. All eight control subjects were between 18 and 55 years of age, were not taking any medications, and were lifelong nonsmokers. There were five males and three females.

Mice

Experimental protocols were approved by the IRB at the University of Colorado Denver, CO. They were in accordance with the protection of animals and the National Institutes of Health guidelines for use of live animals. *miR-223*$^{-/y}$ mice were a gift from V. Dawson (Johns Hopkins University School of Medicine, Baltimore, MD), and wild-type C57BL/6J mice were obtained from the Jackson Laboratory. The *miR-223*$^{-/y}$ mice were generated on a C57BL/6 background. We had received mating pairs of miR-223 knockout mice on the background of C57BL/6 (male, *miR-223*$^{-/y}$; female, *miR-223*$^{-/-}$) and wild-type C57BL/6 mice. Both miR-223 knockout mice and the C57BL/6 mice that served for wild-type control mice have been bred and held in the same specific pathogen-free barrier unit For experiments, *miR-223*$^{-/y}$ and wild-type mice have been matched for age and gender accordingly.

Mouse strains

miR-223$^{-/y}$ mice were generated and first characterized in 2008 (25). The miR-223 locus is located on the X chromosome and is transcribed independently of any known genes. The *miR-223*$^{-/y}$ mice were generated on a C57BL/6 background. These mice are fertile, were bom at normal Mendelian ratios, and do not show any gross abnormalities when maintained in a pathogen-free environment. At the age of 8 to 10 weeks, these mice do not display any pulmonary abnormalities. We received mating pairs of miR-223 knockout mice on a C57BL/6 background (male, *miR-223*$^{-/y}$; female, *miR-223*$^{-/-}$ and wild-type C57BL/6 mice). Both miR-223 knockout mice and the C57BL/6 mice that served for wild-type control

mice have been bred and held in the same specific pathogen-free barrier unit. For experiments, *miR-223*$^{-/y}$ and wild-type mice have been matched for age and gender accordingly.

Murine model for VILI

Murine model for in situ acute VILI was performed as described before (7,20–22). Briefly, acute lung injury was induced with 3 hours of pressure- controlled ventilation using high inspiratory pressure of 45 mbar (2- to 5-mbar positive end-expiratory pressure). For that purpose, animals were anesthetized with pentobarbital [70 mg/kg intraperitoneally (ip) for induction and 20 mg/kg per hour for maintenance] and maintained at stable body temperature using a thermal feedback controller (heating tables and rectal thermometer probes), and fluid was replaced with normal saline (0.05 ml/hour ip). After tracheotomy, a tracheal tube was connected to a mechanical ventilator (Siemens Servo 900C, with pediatric tubing). For all experiments, mice were ventilated in a pressure- controlled ventilation mode with 100% inspired oxygen.

Pulmonary bacterial infection

For *S. aureus* experiments, bacteria were grown, as described previously, and administered by 50 μl of intratracheal inocula at 2×10^8 to 5×10^8 colony-forming units per animal (48). *S. aureus* strains were grown at 37°C to mid-exponential phase OD_{600} (optical density at 600 nm) = 1 (~3 hours) in CCY medium [3% yeast extract, 2% Bacto Casamino adds, 2.3% sodium pyruvate, 0.63% Na_2HPO_4, and 0.041% KH_2PO_4 (pH 6.7)].

Bone marrow chimera

To address the *miR-223* transfer during VILI in vivo, bone marrow mouse chimeras were generated as described previously (7, 49), in which bone marrow was ablated by radiation in wild-type C57BL/6J mice followed by reconstitution with bone marrow derived from *miR-223*$^{-/y}$ (gene-targeted for *miR-223)* and vice versa (*miR-223*$^{-/y}$→wild type and wild type→*miR-223*$^{-/y}$; fig. S4A). Briefly, bone marrow cells harvested from femurs and tibias of euthanized male mice at 8 to 10 weeks of age were transplanted into irradiated (total dose of 2 × 6 gray) recipient mice immediately after irradiation. To monitor transplantation efficiencies, parallel experiments using the same regimen were carried out transplanting CD45.2 bone marrow into irradiated CD45.1 mice, and chimerism was examined by flow cytometric analysis at 6 to 8 weeks after irradiation, correlating with the time of induction of VILI in the experimental chimeric mice (fig. S4B). For this purpose, blood was taken from transplanted recipients; red blood cells were lysed, centrifuged, and resuspended in 200 μl of PBS containing 1% bovine serum albumin (BSA) to determine the percentage of neutrophils expressing CD45.2 in these chimeras (CD45.2→CD45.1); cells were incubated with anti-mouse-CD45.1 antibody (done A20, BioLegend), anti-mouse- CD45.2 antibody (clone 104, eBioscience), anti-mouse-major histocompatibility complex II antibody (clone M5/114.15.2, eBioscience), and anti-mouse-Ly6G antibody (done 1A8, BD Biosciences), and analysis was carried out.

PMN depletion

To deplete neutrophils 24 hours before induction of VILI, mice were given a single dose (1 mg, ip) of Ly6G-specific antibody (1A8, BioXcdl). Control stands for no antibody treatment. These mice received equal volumes of vehide (PBS) at the same time point as the experimental mice received the antibody dose. Flow cytometric analysis demonstrated that depletion was successful (fig. S4, D and E).

Monocyte and macrophage depletion

To deplete monocytes and macrophages 24 hours before induction of VILI, mice were given a combined dose of 100 μl of clodronate liposomes intratracheally plus 200 μl intravenously (ClodronateLiposomes.com). Control mice received equal amounts of control liposomes without dodronate at the same time points.

Closed-chest pulmonary intravital microscopy

Intravital microscopy of the subpleural microvasculature of male wildtype mice was performed as previously described (50). The dye-labeled mimic was purchased from Dharmacon (miRIDIAN Mimic) and was labded with Dy547, a dye with absorbance and emission maximum at 557 and 570 nm, respectively. The mimic-transfected and Calcein-stained HL-60 cells (9×10^6 cells in 200 μl of PBS) were injeded intravenously. After injection and intravital microscopy surgical preparation, mice were ventilated with high tidal volumes. High tidal volume ventilation was continued while performing confocal intravital microscopy using a Nikon AIR microscope with a CFI 75 Apo long working distance 25× objective (numerical aperture, 1.1).

Labeling, intravenous injection of PMN-like cells (HL-60), and visualization by costaining

Neutrophil-like differentiated (4 days with DMSO treatment) HL-60 cells were labded using the Qtracker 655 Labeling Kit (Life Technologies) following the manufacturer's instructions. Thirty minutes before ventilation and induction of acute lung injury, 10 million labded cells were injected retro-orbitally in a total volume of 100 μl per mouse. After induction of VILI, lungs were harvested and paraffin-embedded, and AT-II cells were stained with FITC-pro-SPC. Costaining was analyzed by fluorescence microscopy.

Nanoparticle treatment

To obtain pulmonary overexpression of miR-223, we used a nanopartide- based approach to transport synthetic mmu-*miR-223* into the alveolar space. Neutral lipid emulsion (NLE) consists of 1,2-dioleoyl-sn-glycero- 3-phosphocholine, squalene oil, polysorbate 20, and an antioxidant that, in complex with synthetic miRNAs, form nanopartides in the nanometer diameter range (26). Mice were twice (96 and 48 hours before VILI) given a dose of 20 μg of synthetic mmu-*miR-223* (mimic-223; Dharmacon) or respective control mimic (mimic-ctr) formulated with NLE according to the manufacturer's instructions (MaxSuppressor In Vivo RNA-LANCEr II, Bioo Scientific) by intratracheal injection.

In vivo PARP-1 inhibition

For genetic knockdown of PARP-1 in vivo, 50 μl of saline-formulated high-titer lentiviral shRNA specifically inhibiting PARP-1 (formulated high-titer lentiviral shRNA specifically inhibiting PARP-1, “PARP-1 shRNA”; Sigma-Aldrich) or control lentivirus (empty vector control plasmid DNA that contains no shRNA insert; MISSION pLKO.1-puro Empty Vector Control Plasmid DNA; Sigma-Aldrich) was administered 72 hours before VILI into male miR-223 knockout mice by an intratracheal injection.

BAL and lung tissue harvest

Mice were euthanized after 3 hours of ventilation or no ventilation (control), and lungs were lavaged with 1 ml of sterile PBS (for protein analysis, etc.). After lavage, lungs were perfused with 10 ml of ice-cold saline via the right ventricle to remove any remaining blood in the pulmonary circulation. Lungs were excised and, together with the BAL fluid samples, immediately snap-frozen and stored at −80°C until further processed.

Lung wet-to-dry weight ratio

The lung wet weight-to-dry weight ratios have been performed as described previously.

Microscopic image acquisition

All standard histological images displayed were captured using an Olympus BX51 system microscope supplemented with an Olympus DP72 microscopic digital camera. Images were taken at room temperature using an UPIanApo 10×/0.40 objective lens providing ×100 magnification. For aquisition, cellSens Dimension (version 1.41) from Olympus was used.

Transcriptional analysis

Total RNA or separated fractions of mRNA and miRNA were isolated from human epithelial cells, murine lung tissue, or murine AT-II cells using QIAzol reagent and RNeasy kit following the manufacturer’s instructions (Qiagen). Transcript levels were determined by real-time RT-PCR using specific primer sets (Qiagen). For normalization of expression levels, endogenous expression levels of RNU-6 or SNORD48 or spiked-in cel-miR-39 were used for miRNA studies, and endogenous expression levels of β-actin were used for normalization of all the cytokines (IL-6, IL-1β, CXCL-1, and TNFα), as well as for PARP-1 expression levels.

Isolation of murine alveolar epithelial cells

AT-II cells were purified as described previously (51). Briefly, after induction of VILI, mice were euthanized by pentobarbital overdose. Lungs were lavaged with 3 × 1 ml of sterile PBS and then perfused with ice-cold saline via the right ventricle. As previously described, 3 ml of prewarmed dispase (BD) was instilled, followed by 0.5 ml of a low-melting point agarose, and chest cavity was iced for 2 min to harden the agarose plug. Lungs were removed intact and incubated in 1 ml of dispase at 37°C for 15 min. Tissue was dissociated manually, and cells were filtered (70/40 μm; Thermo Fisher), followed by centrifugation. Pelleted cells were resuspended and labeled with CD45 MicroBeads (Miltenyi Biotec), followed by negative selection using magnetic sorting technology. CD45-negative cells were next treated

with Fc receptor-blocking monoclonal antibody (eBioscience) and labeled with anti-epithelial cell adhesion molecule (EpCAM) biotin (eBioscience) and anti-biotin DyLight 633. EpCAM-positive cells were positively selected using streptavidin magnetic microbeads (Miltenyi). Successful purification of AT-II cells was confirmed by analyzing cells for EpCAM expression using flow cytometric analysis (fig. S4C).

Bronchoalveolar lavage

To obtain BAL fluid after 3 hours of ventilation or from control mice, the tracheal tube was disconnected from the mechanical ventilator, and the lungs were lavaged with 1.0 ml of PBS. All removed fluid was immediately snap-frozen and stored at −80°C for later measurement of the albumin concentration or myeloperoxidase content.

ELISA (albumin, myeloperoxidase, and cytokines) in BAL fluid

BAL fluid samples were thawed to 4°C, and specific protein concentrations in BAL fluid were determined using specific ELISA kits according to the instructions given by the manufacturer: myeloperoxidase (Hycult Biotech) and albumin (Bethyl Laboratories).

Immunoblotting experiments

For detection of PARP-1 protein in cell lysates or murine lung tissue, mouse polyclonal PARP-1 antibodies (C2-10 and B-10; Santa Cruz Biotechnology) were used. For protein loading control, stripped blots were reprobed for β-actin using a mouse monoclonal anti-human β-actin primary antibody (CP01, Calbiochem). Briefly, cell lysate or murine lung tissue-derived protein samples were solubilized in reducing Laemmli sample buffer and heated to 90°C for 5 min. Samples were resolved on a 10% polyacrylamide gel and transferred to nitrocellulose membranes (Trans-Blot Turbo, Bio-Rad). The membranes were blocked for 40 min at room temperature in tris-buffered saline-Tween 20 (TBS-T) supplemented with 2% BSA. The membranes were incubated in 1:1000 mouse polyclonal PARP-1-antibody at 4°C overnight, followed by three 10-min washes in TBS-T. Subsequently, membranes were incubated in 1:5000 goat anti-mouse horseradish peroxidase (ImmunoPure Antibody, Thermo Scientific). After another series of three 10-min washes in TBS-T, proteins were detected by enhanced chemiluminescence (SuperSignal West Femto Maximum Sensitivity Substrate, Thermo Scientific). Protein levels were quantified by densitometry using the ImageJ and Gimp software.

T1α Western blot

Murine BAL fluid was centrifuged at 100,000*g* for 2 hours at 4°C. Pellets were boiled in Laemmli buffer and subjected to Western blotting using an antibody directed against Tlα (Abeam), as previously described and shown to correlate with alveolar epithelial injury.

RAGE ELISA

RAGE levels in the murine BAL fluid were measured by ELISA (R&D) according to the manufacturer’s instructions, as previously described and shown to correlate with epithelial injury.

TUNEL assay

TUNEL staining was performed on lung sections using the In Situ Cell Death Detection Kit (Roche) according to the manufacturer's instructions.

PARP enzyme activity

PARP activity in tissues was measured by an immunohistochemical method assessing PARP activity using biotinylated nicotinamide adenine dinudeotide (NAD) (31). Briefly, cryosections (10 pm) were fixed in 95% ethanol for 10 min at −20°C and then rinsed in PBS. Sections were permeabilized with 1% Triton X-100 in 100 mM tris (pH 8.0) for 15 min at room temperature. Reaction mixture [10 mM $MgCl_2$, 1 mM dithiothreitol, and 30 μM biotinylated NAD^+ in 100 mM tris (pH 8.0)] was then applied to the sections for 30 min at 37°C. Sections incubated with biotinyl-NAD^+-free reaction mixture were used as controls. After three washes in PBS, incorporated biotin was detected by incubation with a 1:200 dilution of each of parts A and B of Vectastain Elite ABC kit (Vector Labs) for 90 min at room temperature. After three 10-min washes in PBS, color was developed with nickel-DAB substrate. Sections were counterstained in Fast Green, dehydrated, and mounted in VectaMount.

Data analysis

All statistical analysis was carried out using GraphPad Prism 5.0. All data are expressed as means ± SEM, and $P < 0.05$ was considered statistically significant. For comparison between two groups, two-sample *t* tests were used. In cases of comparison among more than two groups, ANOVA with Bonferroni correction for multiple comparison adjustments was applied. For all fold change data obtained from real-time quantitative PCR, we took $\log_2$ transformation before performing any statistical analysis. The Mantel-Cox test was used for analysis of survival curves. Because the human data derived from BAL fluid were not normally distributed (confirmed with D'Agostino-Pearson omnibus test; GraphPad Prism 5.0), we report the data as median and 25 to 75% percentiles. The data were analyzed using a nonparametric analysis (Mann-Whitney test).

Supplementary Material

Refer to Web version on PubMed Central for supplementary material.

Acknowledgments

We acknowledge G. P. Downey and M. K. Koeppen for scientific discussions; J. McClendon and E. McNamee for technical assistance; J. M. Poth, M. Hübner, and J. Rink for experimental assistance; P. Soehnlein and A. Schumski for technical advice; I. S. Douglas and D. C. Thompson for providing the MLE-12 and E-10 cell lines; and V. Dawson for providing the *miR*-$223^{-/y}$ mice.

Funding: This work was supported by NIH grants R01-DK097075, R01-HL098294, POI-HL114457, R01-DK082509, R01-HL109233, R01-DK109574, R01-HL119837, and R01-HL133900 (to H.K.E.); NIH grants R01-HL070952 (to M.R.B.) and R01-HL114381 (to P.M.H.); NIH/National Heart, Lung, and Blood Institute Acute Lung Injury Specialized Centers of Clinically Oriented Research grant P50 HL074024 (to T.J.S.); NIH grants HL080396 and ES023384 (to C.M.E.) and HL130938 (to C.M.E. and W.J.J.); a grant from the German National Research Foundation [Deutsche Forschungsgemeinschaft (DFG), SFB815] (to K.Z.); a grant from the Crohn's and Colitis Foundation of America and North American Society for Pediatric Gastroenterology, Hepatology, and Nutrition (to J.C.M.); grants from the DFG and the American Heart Association (AHA) (to V.N.); and from the AHA (to E.T.C, C.M.E, and T.W.).

REFERENCES AND NOTES

1. ARDS Definition Task Force. Ranieri VM, Rubenfeld GD, Thompson BT, Ferguson ND, Caldwell E, Fan E, Camporota L, Slutsky AS. Acute respiratory distress syndrome: The Berlin Definition. JAMA. 2012; 307:2526–2533. [PubMed: 22797452]
2. Ware LB, Matthay MA. The acute respiratory distress syndrome. N Engl J Med. 2000; 342:1334–1349. [PubMed: 10793167]
3. Eckle T, Koeppen M, Eltzschig HK. Role of extracellular adenosine in acute lung injury. Physiology (Bethesda). 2009; 24:298–306. [PubMed: 19815856]
4. Dengler V, Downey GP, Tuder RM, Eltzschig HK, Schmidt EP. Neutrophil intercellular communication in acute lung injury: Emerging roles of microparticles and gap junctions. Am J Respir Cell Mol Biol. 2013; 49:1–5. [PubMed: 23815257]
5. Schingnitz U, Hartmann K, MacManus CF, Eckle T, Zug S, Colgan SP, Eltzschig HK. Signaling through the A2B adenosine receptor dampens endotoxin-induced acute lung injury. J Immunol. 2010; 184:5271–5279. [PubMed: 20348420]
6. Ehrentraut H, Clambey ET, McNamee EN, Brodsky KS, Ehrentraut SF, Poth JM, Riegel AK, Westrich JA, Colgan SP, Eltzschig HK. $CD73^{+}$ regulatory T cells contribute to adenosine-mediated resolution of acute lung injury. FASEB J. 2013; 27:2207–2219. [PubMed: 23413361]
7. Eckle T, Grenz A, Laucher S, Eltzschig HK. A2B adenosine receptor signaling attenuates acute lung injury by enhancing alveolar fluid clearance in mice. J Clin Invest. 2008; 118:3301–3315. [PubMed: 18787641]
8. Eckle T, Füllbier L, Wehrmann M, Khoury J, Mittelbronn M, Ibla J, Rosenberger P, Eltzschig HK. Identification of ectonucleotidases CD39 and CD73 in innate protection during acute lung injury. J Immunol. 2007; 178:8127–8137. [PubMed: 17548651]
9. Théry C, Ostrowski M, Segura E. Membrane vesicles as conveyors of immune responses. Nat Rev Immunol. 2009; 9:581–593. [PubMed: 19498381]
10. Small EM, Olson EN. Pervasive roles of microRNAs in cardiovascular biology. Nature. 2011; 469:336–342. [PubMed: 21248840]
11. Friedman RC, Farh KKH, Burge CB, Bartel DP. Most mammalian mRNAs are conserved targets of microRNAs. Genome Res. 2009; 19:92–105. [PubMed: 18955434]
12. Mittelbrunn M, Sánchez-Madrid F. Intercellular communication: Diverse structures for exchange of genetic information. Nat Rev Mol Cell Biol. 2012; 13:328–335. [PubMed: 22510790]
13. Campbell EL, Bruyninckx WJ, Kelly CJ, Glover LE, McNamee EN, Bowers BE, Bayless AJ, Scully M, Saeedi BJ, Golden-Mason L, Ehrentraut SF, Curtis VF, Burgess A, Garvey JF, Sorensen A, Nemenoff R, Jedlicka P, Taylor CT, Kominsky DJ, Colgan SP. Transmigrating neutrophils shape the mucosal microenvironment through localized oxygen depletion to influence resolution of inflammation. Immunity. 2014; 40:66–77. [PubMed: 24412613]
14. Ward JR, Heath PR, Catto JW, Whyte MKB, Milo M, Renshaw SA. Regulation of neutrophil senescence by microRNAs. PLOS ONE. 2011; 6:e15810. [PubMed: 21283524]
15. Faigle M, Seessle J, Zug S, El Kasmi KC, Eltzschig HK. ATP release from vascular endothelia occurs across Cx43 hemichannels and is attenuated during hypoxia. PLOS ONE. 2008; 3:e2801. [PubMed: 18665255]
16. Kuhlicke J, Frick JS, Morote-Garcia JC, Rosenberger P, Eltzschig HK. Hypoxia inducible factor (HIF)-1 coordinates induction of Toll-like receptors TLR2 and TLR6 during hypoxia. PLOS ONE. 2007; 2:e1364. [PubMed: 18159247]
17. Brinkmann V, Reichard U, Goosmann C, Fauler B, Uhlemann Y, Weiss DS, Weinrauch Y, Zychlinsky A. Neutrophil extracellular traps kill bacteria. Science. 2004; 303:1532–1535. [PubMed: 15001782]
18. Yumoto R, Nishikawa H, Okamoto M, Katayama H, Nagai J, Takano M. Clathrin-mediated endocytosis of FITC-albumin in alveolar type II epithelial cell line RLE-6TN. Am J Physiol Lung Cell Mol Physiol. 2006; 290:L946–L955. [PubMed: 16361359]
19. Ikehata M, Yumoto R, Nakamura K, Nagai J, Takano M. Comparison of albumin uptake in rat alveolar type II and type I-like epithelial cells in primary culture. Pharm Res. 2008; 25:913–922. [PubMed: 17851738]

20. Eckle T, Hughes K, Ehrentraut H, Brodsky KS, Rosenberger P, Choi DS, Ravid K, Weng T, Xia Y, Blackburn MR, Eltzschig HK. Crosstalk between the equilibrative nucleoside transporter ENT2 and alveolar Adora2b adenosine receptors dampens acute lung injury. FASEB J. 2013; 27:3078–3089. [PubMed: 23603835]
21. Koeppen M, McNamee EN, Brodsky KS, Aherne CM, Faigle M, Downey GP, Colgan SP, Evans CM, Schwartz DA, Eltzschig HK. Detrimental role of the airway mucin Muc5ac during ventilator-induced lung injury. Mucosal Immunol. 2013; 6:762–775. [PubMed: 23187315]
22. Eckle T, Füllbier L, Grenz A, Eltzschig HK. Usefulness of pressure-controlled ventilation at high inspiratory pressures to induce acute lung injury in mice. Am J Physiol Lung Cell Mol Physiol. 2008; 295:L718–L724. [PubMed: 18708630]
23. Kim JH, Suk MH, Yoon DW, Kim HY, Jung KH, Kang EH, Lee SY, Lee SY, Suh IB, Shin C, Shim JJ, In KH, Yoo SH, Kang KH. Inflammatory and transcriptional roles of poly (ADP-ribose) polymerase in ventilator-induced lung injury. Crit Care. 2008; 12:R108. [PubMed: 18718025]
24. Streppel MM, Pai S, Campbell NR, Hu C, Yabuuchi S, Canto MI, Wang JS, Montgomery EA, Maitra A. MicroRNA 223 is upregulated in the multistep progression of Barrett's esophagus and modulates sensitivity to chemotherapy by targeting. PARP1 Clin Cancer Res. 2013; 19:4067–4078. [PubMed: 23757351]
25. Johnnidis JB, Harris MH, Wheeler RT, Stehling-Sun S, Lam MH, Kirak O, Brummelkamp TR, Fleming MD, Camargo FD. Regulation of progenitor cell proliferation and granulocyte function by microRNA-223. Nature. 2008; 451:1125–1129. [PubMed: 18278031]
26. Trang P, Wiggins JF, Daige CL, Cho C, Omotola M, Brown D, Weidhaas JB, Bader AG, Slack FJ. Systemic delivery of tumor suppressor microRNA mimics using a neutral lipid emulsion inhibits lung tumors in mice. Mol Ther. 2011; 19:1116–1122. [PubMed: 21427705]
27. Fazi F, Rosa A, Fatica A, Gelmetti V, De Marchis ML, Nervi C, Bozzoni I. A minicircuitry comprised of microRNA-223 and transcription factors NFI-A and C/EBPα regulates human granulopoiesis. Cell. 2005; 123:819–831. [PubMed: 16325577]
28. Pulikkan JA, Dengler V, Peramangalam PS, Peer Zada AA, Müller-Tidow C, Bohlander SK, Tenen DG, Behre G. Cell-cycle regulator E2F1 and microRNA-223 comprise an autoregulatory negative feedback loop in acute myeloid leukemia. Blood. 2010; 115:1768–1778. [PubMed: 20029046]
29. Fukao T, Fukuda Y, Kiga K, Sharif J, Hino K, Enomoto Y, Kawamura A, Nakamura K, Takeuchi T, Tanabe M. An evolutionarily conserved mechanism for microRNA-223 expression revealed by microRNA gene profiling. Cell. 2007; 129:617–631. [PubMed: 17482553]
30. Ba X, Garg NJ. Signaling mechanism of poly(ADP-ribose) polymerase-1 (PARP-1) in inflammatory diseases. Am J Pathol. 2011; 178:946–955. [PubMed: 21356345]
31. Liaudet L, Pacher P, Mabley JG, Virág L, Soriano FG, Haskó G, Szabó C. Activation of poly(ADP-Ribose) polymerase-1 is a central mechanism of lipopolysaccharide-induced acute lung inflammation. Am J Respir Crit Care Med. 2002; 165:372–377. [PubMed: 11818323]
32. Zingarelli B, Hake PW, O'Connor M, Denenberg A, Wong HR, Kong S, Aronow BJ. Differential regulation of activator protein-1 and heat shock factor-1 in myocardial ischemia and reperfusion injury: Role of poly(ADP-ribose) polymerase-1. Am J Physiol Heart Circ Physiol. 2004; 286:H1408–H1415. [PubMed: 14670820]
33. Jijon HB, Churchill T, Malfair D, Wessler A, Jewell LD, Parsons HG, Madsen KL. Inhibition of poly(ADP-ribose) polymerase attenuates inflammation in a model of chronic colitis. Am J Physiol Gastrointest Liver Physiol. 2000; 279:G641–G651. [PubMed: 10960365]
34. Gasser O, Schifferli JA. Activated polymorphonuclear neutrophils disseminate anti-inflammatory microparticles by ectocytosis. Blood. 2004; 104:2543–2548. [PubMed: 15213101]
35. Eken C, Martin PJ, Sadallah S, Treves S, Schaller M, Schifferli JA. Ectosomes released by polymorphonuclear neutrophils induce a MerTK-dependent anti-inflammatory pathway in macrophages. J Biol Chem. 2010; 285:39914–39921. [PubMed: 20959443]
36. Zemans RL, McClendon J, Aschner Y, Briones N, Young SK, Lau LF, Kahn M, Downey GP. Role of β-catenin-regulated CCN matricellular proteins in epithelial repair after inflammatory lung injury. Am J Physiol Lung Cell Mol Physiol. 2013; 304:L415–L427. [PubMed: 23316072]
37. Matthay MA, Ware LB, Zimmerman GA. The acute respiratory distress syndrome. J Clin Invest. 2012; 122:2731–2740. [PubMed: 22850883]

38. Grommes J, Soehnlein O. Contribution of neutrophils to acute lung injury. Mol Med. 2011; 17:293–307. [PubMed: 21046059]
39. Abraham E, Carmody A, Shenkar R, Arcaroli J. Neutrophils as early immunologic effectors in hemorrhage- or endotoxemia-induced acute lung injury. Am J Physiol Lung Cell Mol Physiol. 2000; 279:L1137–L1145. [PubMed: 11076804]
40. Folkesson HG, Matthay MA, Hébert CA, Broaddus VC. Acid aspiration-induced lung injury in rabbits is mediated by interleukin-8-dependent mechanisms. J Clin Invest. 1995; 96:107–116. [PubMed: 7615779]
41. Kühl AA, Kakirman H, Janotta M, Dreher S, Cremer P, Pawlowski NN, Loddenkernper C, Heimesaat MM, Grollich K, Zeitz M, Farkas S, Hoffmann JC. Aggravation of different types of experimental colitis by depletion or adhesion blockade of neutrophils. Gastroenterology. 2007; 133:1882–1892. [PubMed: 18054560]
42. Schlegel R, Dickson RB, Willingham MC, Pastan IH. Amantadine and dansylcadaverine inhibit vesicular stomatitis virus uptake and receptor-mediated endocytosis of alpha 2-macroglobulin. Proc Natl Acad Sci USA. 1982; 79:2291–2295. [PubMed: 6179094]
43. Zhang X, Goncalves R, Mosser DM. The isolation and characterization of murine macrophages. Curr Protoc Immunol. 2008 **Chapter 14**, Unit 14.1.
44. Reutershan J, Morris MA, Burcin TL, Smith DF, Chang D, Saprito MS, Ley K. Critical role of endothelial CXCR2 in LPS-induced neutrophil migration into the lung. J Clin Invest. 2006; 116:695–702. [PubMed: 16485040]
45. Yang Y-L, Tang GJ, Wu YL, Yien HW, Lee TS, Kou YR. Exacerbation of wood smoke-induced acute lung injury by mechanical ventilation using moderately high tidal volume in mice. Respir Physiol Neurobiol. 2008; 160:99–108. [PubMed: 17964866]
46. Mosser DM, Zhang X. Activation of murine macrophages. Curr Protoc Immunol. 2008 **Chapter 14**, Unit 14.2.
47. Gupta AK, Giaglis S, Hasler P, Hahn S. Efficient neutrophil extracellular trap induction requires mobilization of both intracellular and extracellular calcium pools and is modulated by cyclosporine A. PLOS ONE. 2014; 9:e97088. [PubMed: 24819773]
48. Labandeira-Rey M, Couzon F, Boisset S, Brown EL, Bes M, Benito Y, Barbu EM, Vazquez V, Höök M, Etienne J, Vandenesch F, Bowden MG. Staphylococcus aureus Panton-Valentine leukocidin causes necrotizing pneumonia. Science. 2007; 315:1130–1133. [PubMed: 17234914]
49. Eckle T, Faigle M, Grenz A, Laucher S, Thompson LF, Eltzschig HK. A2B adenosine receptor dampens hypoxia-induced vascular leak. Blood. 2008; 111:2024–2035. [PubMed: 18056839]
50. Schmidt EP, Yang Y, Janssen WJ, Gandjeva A, Perez MJ, Barthel L, Zemans RL, Bowman JC, Koyanagi DE, Yunt ZX, Smith LP, Cheng SS, Overdier KH, Thompson KR, Geraci MW, Douglas IS, Pearse DB, Tuder RM. The pulmonary endothelial glycocalyx regulates neutrophil adhesion and lung injury during experimental sepsis. Nat Med. 2012; 18:1217–1223. [PubMed: 22820644]
51. Messier EM, Mason RJ, Kosmider B. Efficient and rapid isolation and purification of mouse alveolar type II epithelial cells. Exp Lung Res. 2012; 38:363–373. [PubMed: 22888851]

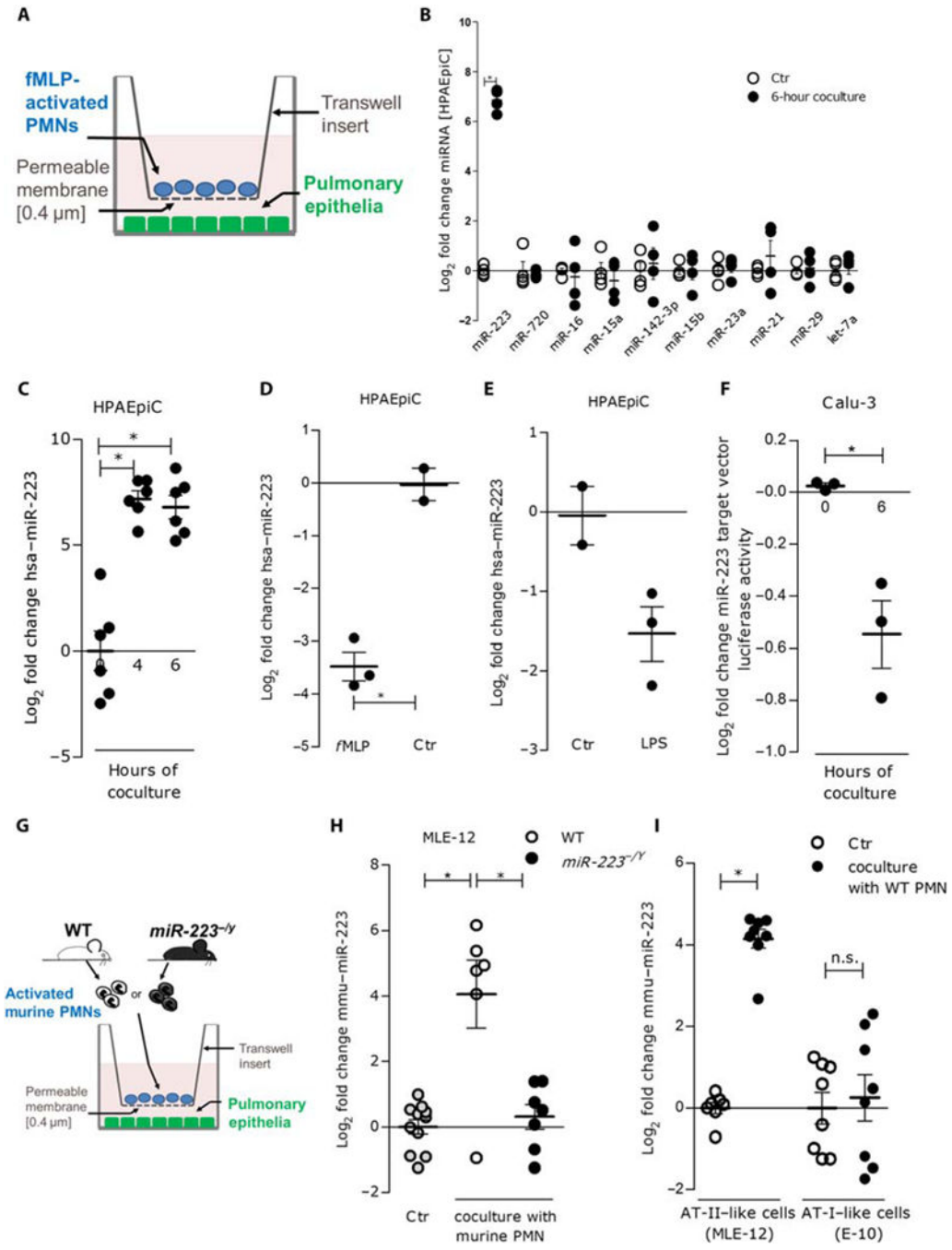

Fig. 1. Transfer of *miR-223* during neutrophil-epithelial cell interactions

(**A**) Coculture setup for human neutrophils (PMNs) and human pulmonary epithelial cells. (**B**) Expression of miRNA in human epithelial cells after coculture of HPAEpiC with activated human PMNs (means ± SEM; $n = 4$). (**C**) hsa-*miR-223* expression after coculture of HPAEpiC with activated human PMNs (means ± SEM; $n=6$). (**D** and **E**) Expression of *miR-223* in HPAEpiC after exposure of HPAEpiC cells to (D) *f*MLP or (E) LPS [means ± SEM; $n=2$ for control (Ctr) group or $n = 3$ for *f*MLP and LPS groups]. (**F**) Epithelial cell *miR-223* target vector luciferase activity after coculture of activated human PMNs with

transfected pulmonary epithelial cells (Calu-3); data are normalized to control vector activity and compared to no coculture (means ± SEM; $n = 3$ independent experiments). (**G**) Setup for murine coculture. (**H**) mmu-*miR-223* expression in mouse pulmonary epithelial (MLE-12) cells after coculture with activated murine PMNs derived from wild-type (WT) or *miR-223*$^{-/y}$ mice (means ± SEM; $n = 11$ for the control group, $n = 6$ for mouse WT PMNs, and $n = 7$ for *miR-223*$^{-/y}$ PMNs). (**I**) mmu-*miR-223* expression in MLE-12 cells or E-10 cells after coculture with activated murine PMNs (means ± SEM; $n = 7$ for MLE-12 control group or $n = 8$ for all other conditions) [$*P < 0.05$, Student's *t* test or analysis of variance (ANOVA)]. n.s., not significant.

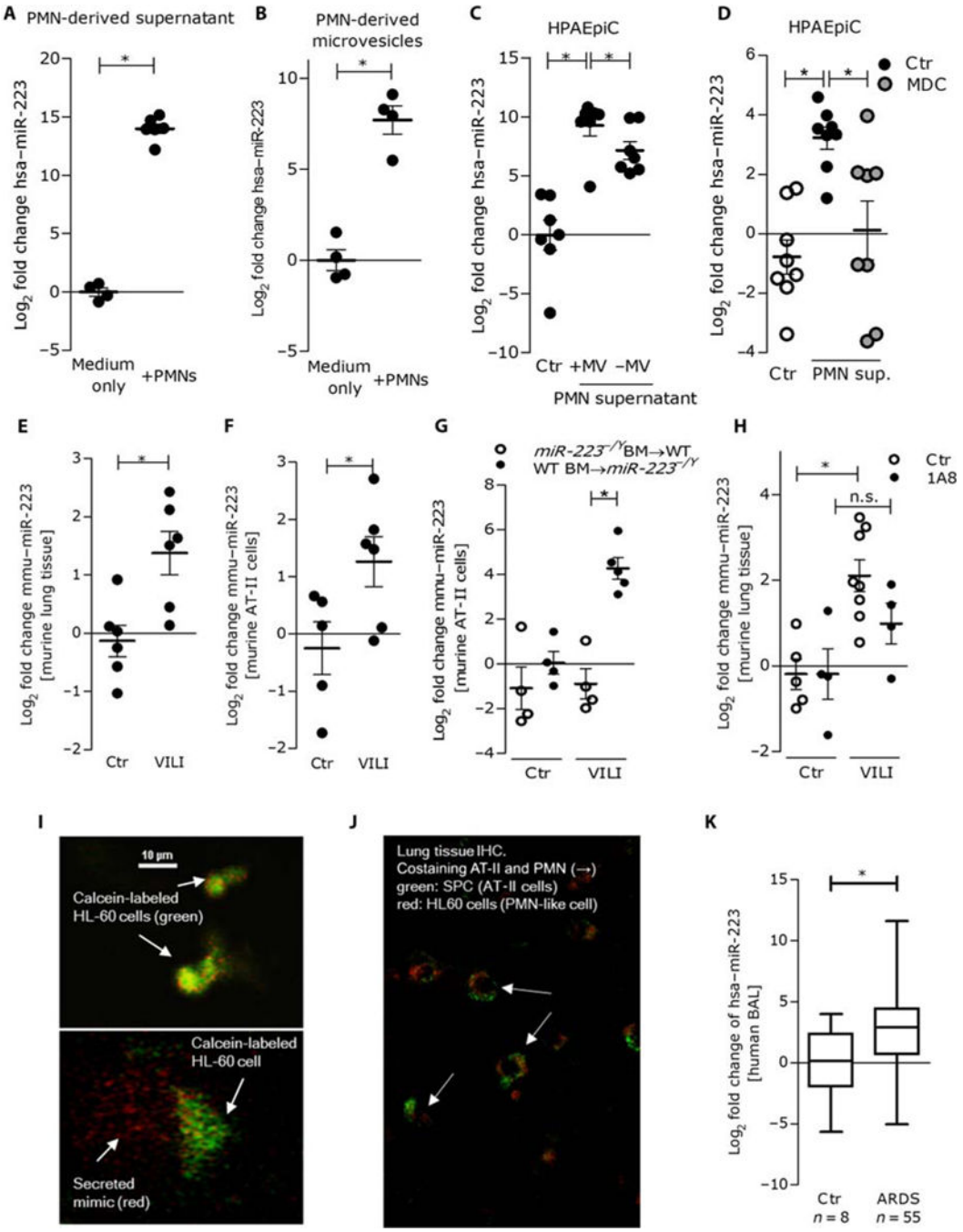

Fig. 2. PMN-dependent transfer of *miR-223* to human pulmonary epithelial cells

(**A**) hsa-*miR*-223 release into human PMN–derived supernatants was compared to culture medium only (means ± SEM; $n = 4$ in the culture medium–only group and $n = 6$ in the PMN-derived supernatant group) after human PMN activation. **(B)** hsa-*miR-223* in PMN supernatant–derived microvesicles compared to medium only (means ± SEM; $n = 4$). **(C)** Expression of *miR-223* in HPAEpiC cells after incubation with PMN-derived or control supernatants containing microvesicles (+MV) or depleted of microvesicles (−MV) (means ± SEM; $n = 7$). **(D)** hsa-*miR-223* expression after coculture of activated human PMNs with

HPAEpiC cells in the presence or absence of the endocytosis inhibitor monodansylcadaverine (MDC) (means ± SEM; $n = 8$). **(E)** Pulmonary expression of mmu-*miR-223* in a mouse model of VILI (means ± SEM; $n = 6$ mice per group). **(F)** mmu-*miR-223* expression in isolated mouse AT-II cells after VILI (means ± SEM; $n = 5$ mice in the control group and $n = 6$ mice in the VILI group). **(G)** mmu-*miR-223* expression in AT-II cells Isolated from a mouse bone marrow (BM) chimera (WT → *miR-223*$^{-/y}$ and *miR-223*$^{-/y}$ → WT) after exposure to VILI (means ± SEM; $n = 5$ mice in the WT → *miR-223*$^{-/y}$ VILI group and $n = 4$ mice in all other groups). **(H)** mmu-*miR-223* expression in murine lung tissue during VILI after antibody-mediated depletion of PMNs (means ± SEM; $n = 5$ mice in the control-treated group, $n = 4$ mice in the 1A8 antibody-treated group, and $n = 7$ mice in the control-treated VILI group). **(I)** Intravital microscopy of HL-60 cells, transfected with a dye-labeled miRNA mimic (red) and labeled with calcein dye (green), after intravenous injection into mice ventilated for 30 min (top) or after 90 min of high tidal ventilation to induce VILI (bottom) (two representative images; $n = 3$ mice). **(J)** Immunohistochemical (IHC) costaining of AT-II cells [fluorescein isothiocyanate (FITC)–pro–surfactant protein C (SPC); green] and Qtracker-labeled and intravenously injected HL-60 cells (Qtracker-655; red) in murine lung tissue after induction of VILI (one representative image; $n = 3$ mice). **(K)** hsa-*miR-223* expression in BAL fluid derived from patients with ARDS or healthy controls (median and 25 to 75% percentiles; $n = 8$ controls and $n = 55$ ARDS patients; Table 1) (*$P < 0.05$, Student's *t* test, ANOVA, or nonparametric analysis Mann-Whitney test).

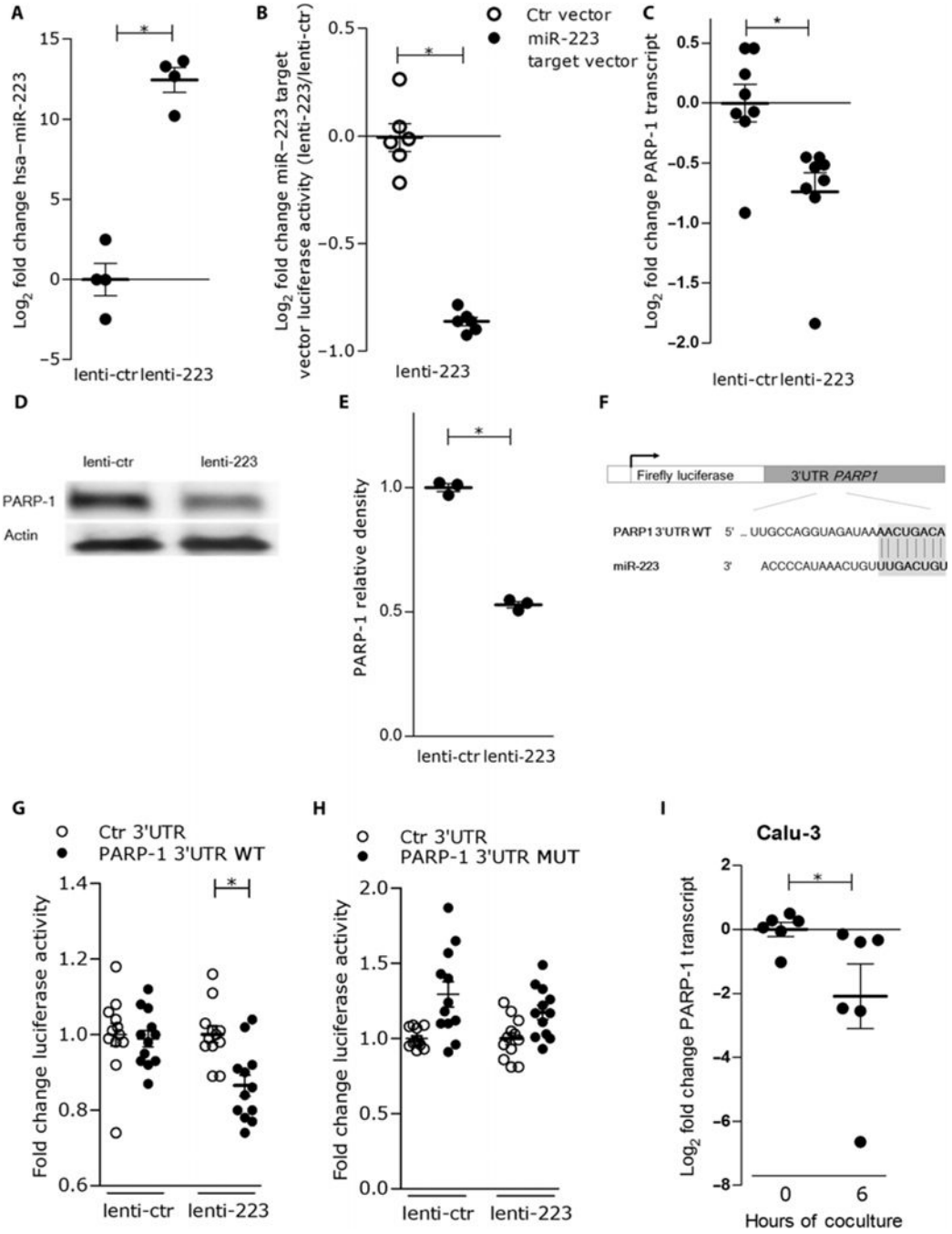

Fig. 3. PARP-1 is a *miR-223* gene target in human pulmonary epithelial cells

(**A**) Baseline hsa-*miR-223* expression in lentiviral-transduced, human Calu-3 (lenti-223) cells compared to control Calu-3 (lenti-ctr) cells (means ± SEM; n=4). **(B)** Epithelial cell *miR-223* target vector luciferase activity in transfected human Calu-3 cells compared to control vector activity (means ± SEM; n=6). **(C)** Analysis of PARP-1 transcripts in lentiviral-transduced human Calu-3 cells compared to control Calu-3 cells using real-time reverse transcription polymerase chain reaction (RT-PCR) relative to the housekeeping gene β-actin (means ± SEM; n = 8). **(D** and **E)** Western blot analysis of PARP-1 protein in

lentiviral-transduced human Calu-3 cells compared to control Calu-3 cells (one representative blot of three is shown; quantification by densitometry, n=3). **(F)** Schematic of luciferase reporter plasmids showing the binding sequence between PARP-1 3′UTR and hsa-*miR*-223. **(G** and **H)** Luciferase activities of PARP-1 3′UTR WT plasmid or mutated (MUT) plasmid compared to control 3′UTR plasmid after transfection into lentiviral-transduced human Calu-3 cells (lentl-ctr or lentl-223) (means ± SEM; n=12). **(I)** PARP-1 transcripts in the human Calu-3 cell line after coculture with human PMNs measured by real-time RT-PCR relative to the housekeeping gene β-actin (means ± SEM; n = 6) (*P < 0.05; Student's t test).

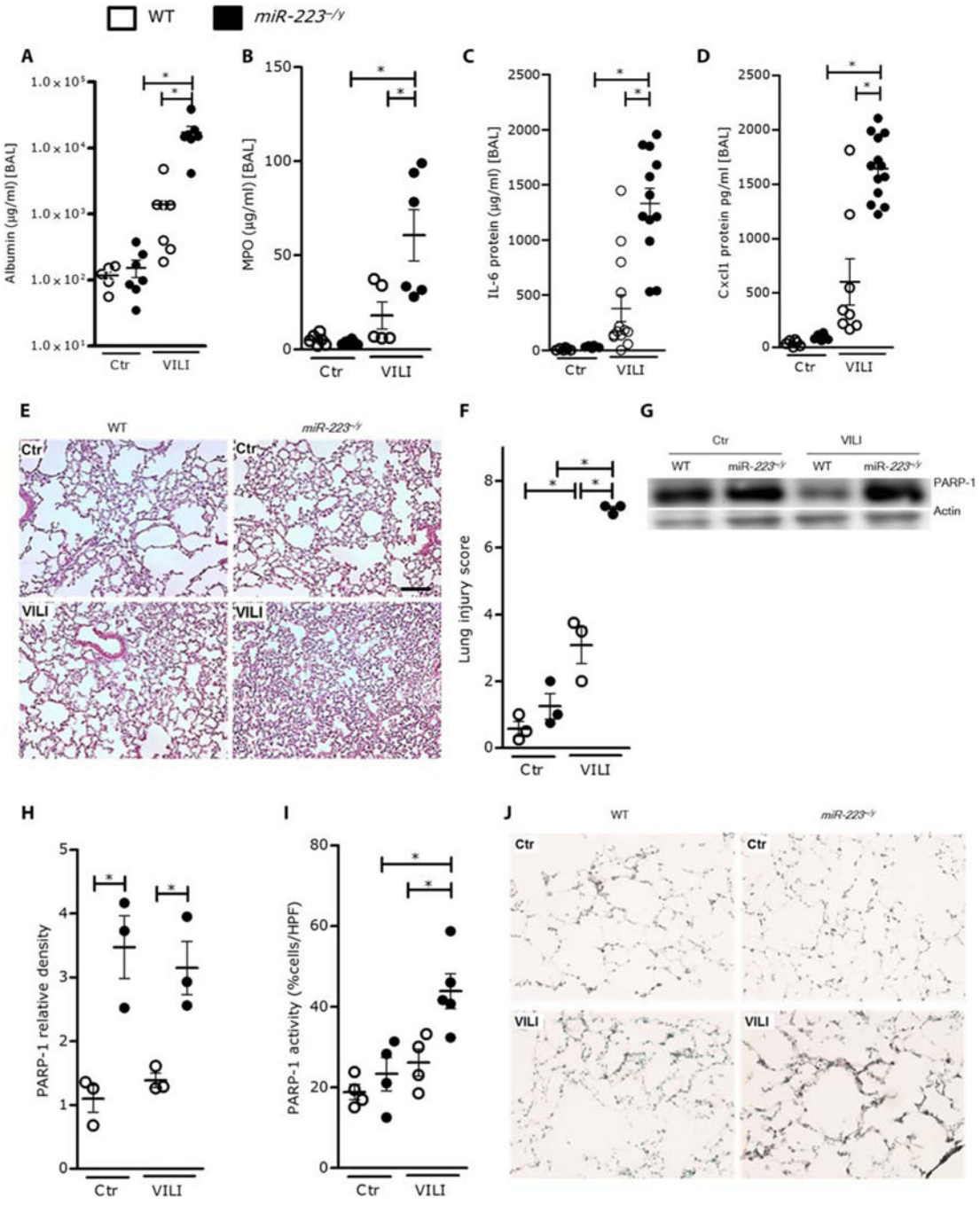

Fig. 4. Acute lung injury in *miR-223*$^{-/y}$ mice

WT and *miR-223*$^{-/y}$ mice were exposed to VILI, **(A)** Albumin detected in mouse BAL fluid was measured in WT and *miR-223*$^{-/y}$ mice (means ± SEM; n=5 mice in the WT control group and n=7 mice in all others groups). **(B)** The neutrophil enzyme myeloperoxidase (MPO) was measured in BAL fluid from WT and *miR-223*$^{-/y}$ mice (means ± SEM; n = 5 mice in the WT VILI group and n = 6 mice in all others groups). (**C** and **D) I**nterleukin-6 (IL-6) and Cxcl-1 protein concentrations in BAL fluid from WT and *miR-223*$^{-/y}$ mice were measured by enzyme-linked immunosorbent assay (ELISA) [means ± SEM; **(C)** n = 6 mice

in the control group, n =13 mice in the WTVILI group, and n = 12 mice in the *miR*-223$^{-/y}$ VILI group; **(D)** n=6 mice in the control group, n=8 mice in the WTVILI group, and n = 13 mice in the *miR-223*$^{-/y}$ VILI group]. **(E)** Representative slides of pulmonary histology for WT and *miR-223*$^{-/y}$ mice [hematoxylin and eosin (H&E) staining]. Scale bar, 100 μm. **(F)** Scoring of lung injury in slides from (E). (**G** and **H)** Pulmonary PARP-1 protein expression In WT or *miR-223*$^{-/y}$ mice at baseline (Ctr) or during acute lung Injury (VILI) relative to the housekeeping gene β-actin (one representative blot of three is shown; quantification by densitometry, n = 3). **(I)** PARP-1 enzyme activity in WT or *miR-223*$^{-/y}$ mice (n = 5 mice in the *miR-223*$^{-/y}$ VILI group or n = 4 mice for all other groups). HPF, high-power field. **(J)** Representative immunohistochemical staining for PARP-1 activity in WT and *miR-223*$^{-/y}$ mice (*P < 0.05, ANOVA).

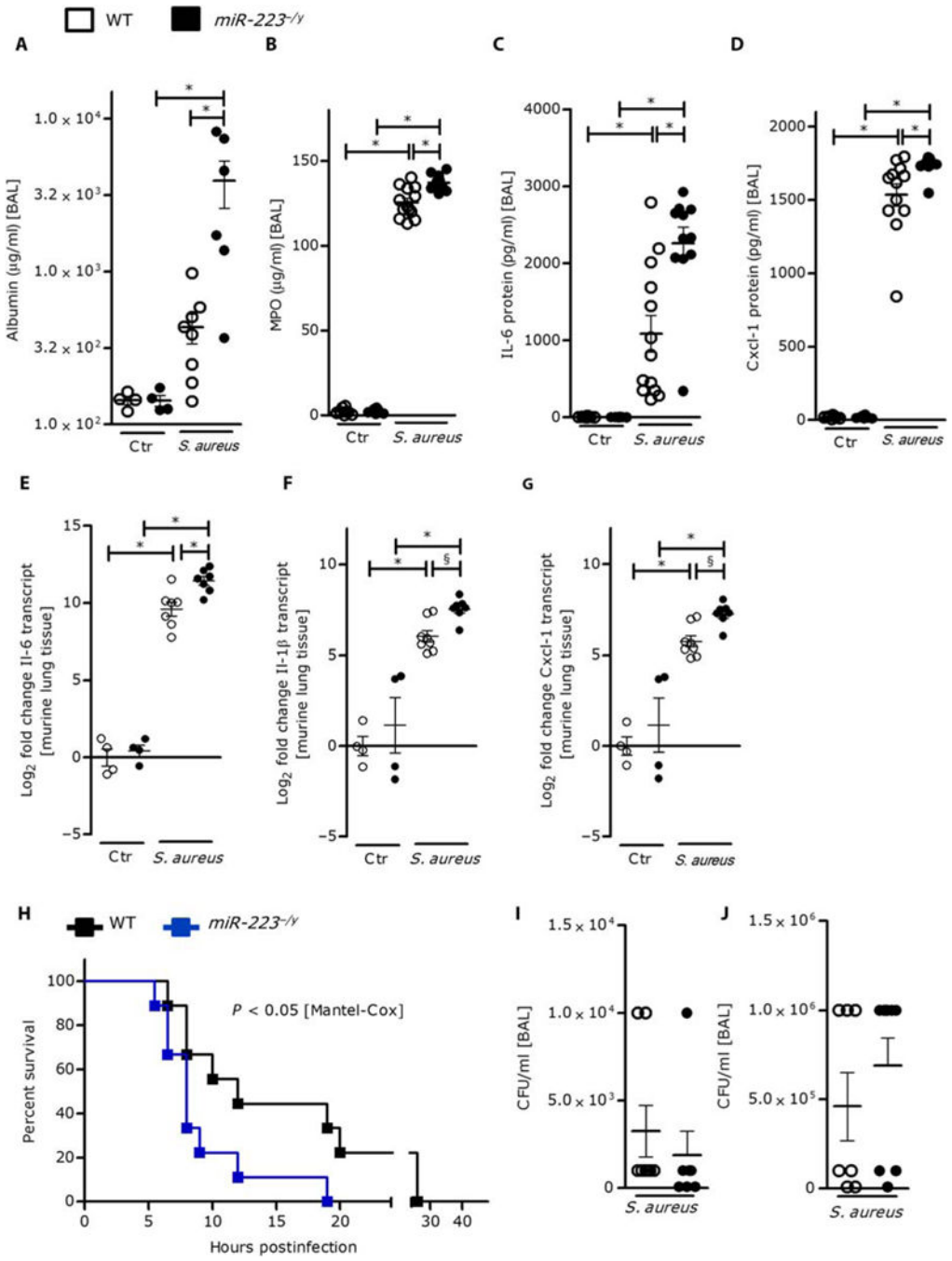

Fig. 5. Pulmonary bacterial Infection in *miR*$^{-/y}$ mice

Pulmonary Infection in *miR-223*$^{-/y}$ mice (filled circles) and WT mice (empty circles) was induced by intratracheal administration of *S. aureus*. **(A)** Albumin detected in the BAL fluid was measured [(means ± SEM; $n = 4$ mice in the control group, $n = 8$ mice in the WT group Infected with *S. aureus*, and $n = 6$ mice in the *miR*-223$^{-/y}$ group infected with *S. aureus*]. **(B)** Myeloperoxidase was measured in BAL fluid from *miR-223*$^{-/y}$ mice infected with *S. aureus*. IL-6 and Cxcl-1 proteins were measured in BAL fluid using ELISA: **(C)** IL-6 and **(D)** Cxcl-1 [(**B** and **C**) means ± SEM; $n = 8$ mice in the control group, $n = 13$ mice in the

WT group infected with *S. aureus*, and $n = 11$ mice in the *miR-223*$^{-/y}$ group infected with *S. aureus*; **(D)** means ± SEM; $n = 8$ mice in the control group, $n = 12$ mice in the WT mouse group infected with *S. aureus*, $n = 11$ mice in the *miR-223*$^{-/y}$ group infected with *S. aureus*). Transcripts were analyzed in mouse lung tissue for **(E)** IL-6, **(F)** IL-1β, and **(G)** Cxd-1 by real-time RF-PCR relative to the housekeeping gene β-actin. [(E) means ± SEM; $n = 4$ WT or *miR-223*$^{-/y}$ mice in the control groups and $n = 7$ WT or *miR-223*$^{-/y}$ mice in the *S. aureus* infection groups; (**F** and **C**) means ± SEM; $n = 4$ WT or *miR-223*$^{-/y}$ mice in the control groups, $n = 8$ mice in the WT *S. aureus* infection groups, and $n = 7$ in the *miR-223*$^{-/y}$ *S. aureus* infection group]. **(H)** Survival of WT and *miR-223*$^{-/y}$ mice after pulmonary infection with *S. aureus* bacteria ($n = 9$ mice per group). Number of bacterial colony-forming units (CFU) 4 hours after infection with intratracheal *S. aureus* **(I)** (means ± SEM; $n = 8$ mice in the WT group and $n = 7$ mice in the *miR-223*$^{-/y}$ group) and in BAL fluid when mice were moribund **(J)** (means ± SEM; $n = 7$ mice in the WT group and $n = 9$ mice in the *miR-223*$^{-/y}$ group) ($^{*}P < 0.05$ and $^{\S}P < 0.05$ in the post hoc analysis between WT mice and *miR-223*$^{-/y}$ mice after *S. aureus* exposure).

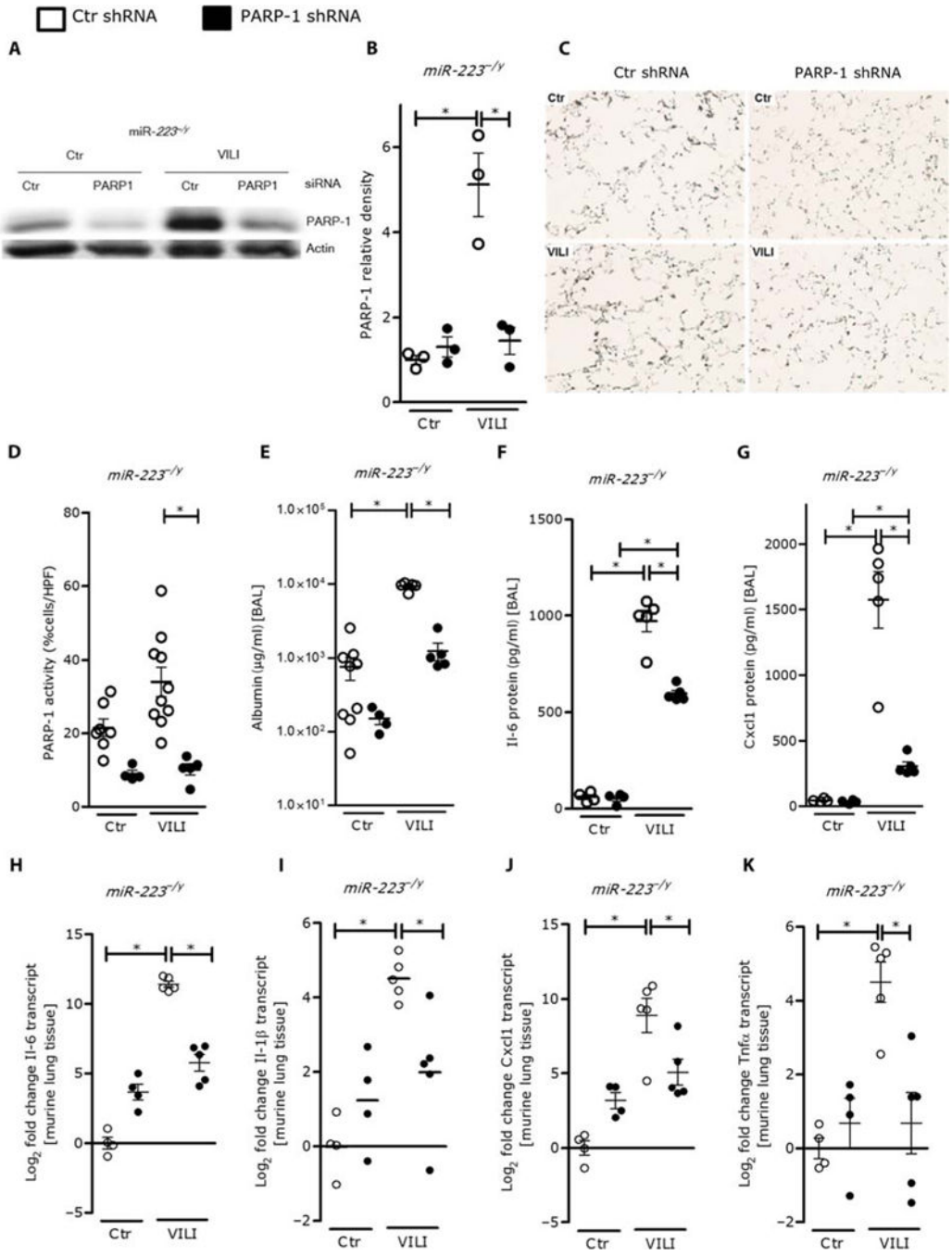

Fig. 6. Genetic knockdown of PARP-1 with shRNA in *miR-223*$^{-/y}$ mice with acute lung injury

(**A** and **B**) Pulmonary PARP-1 protein knockdown in *miR-223*$^{-/y}$ mice using PARP-1 shRNA [one representative blot of three is shown; quantification by densitometry in (B), means ± SEM; $n = 3$ mice]. **(C)** Immunohistochemical staining for pulmonary PARP-1 activity in *miR-223*$^{-/y}$ mice treated with Parp-1 shRNA or control shRNA ($n = 3$ mice). (**D**) Quantification of immunohistochemical staining in (C) [means ± SEM; $n = 6$ mice in the nonventilated control shRNA group, $n = 4$ in the nonventilated *Parp-1* shRNA group, and $n =$ 10 or 5 mice in the control shRNA or *Parp-1* shRNA ventilated (VILI) groups]. **(E)** Albumin

detected In BAL fluid in *miR-223*$^{-/y}$ mice treated with control or *Parp-1* shRNA and cytokine concentrations in BAL fluid measured by ELISA **(F)** IL-6 and **(G)** Cxcl-1 protein. Pulmonary transcripts in *miR-223*$^{-/y}$ mice treated with control or Parp-1 shRNA for **(H)** IL-6, **(I)** IL-1β, **(J)** Cxcl-1, and **(K)** tumor necrosis factor-α (Tnfα), assessed by RT-PCR relative to the housekeeping β-actin gene [(F to K) means ± SEM; $n = 4$ mice in the control groups and $n = 5$ mice in the VILI groups] (*$P < 0.05$, ANOVA).

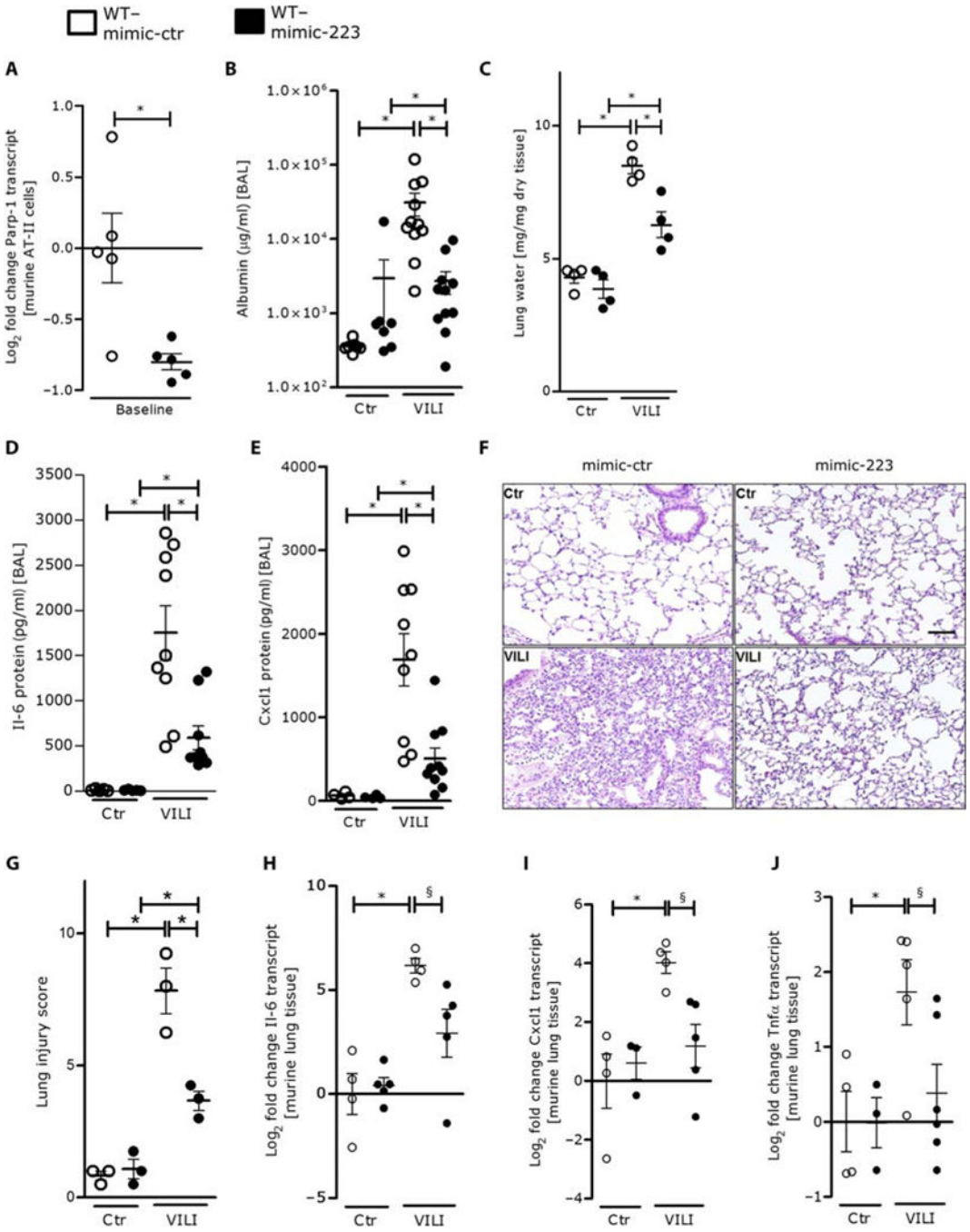

Fig. 7. Pulmonary overexpression of *miR-223* during acute lung injury in WT mice

Nanoparticle-mediated overexpression of *mmu-miR-223* in C57BL/6J mice before acute lung injury induced by ventilation (VILI). **(A)** Parp-1 transcripts measured by real-time RT-PCR relative to the housekeeping gene β-actin in isolated murine AT-II cells before and after nanoparticle-mediated delivery of *miR-223* mimic (either mimic-control or mimic-223) (means ± SEM; $n = 5$ mice per group). **(B)** Albumin detection in murine BAL fluid was assessed by ELISA in nanoparticle-treated WT mice (nanoparticles contained either *miR-223* mimic or control mimic; means ± SEM; $n = 7$ mice in the control groups and $n =$

11 mice in the acute lung injury groups). **(C)** Lung wet–to–dry weight ratio of nanoparticle-treated murine lungs at baseline and after acute lung injury induced by ventilation (VILI) (means ± SEM; $n = 4$ mice per group). **(D** and **E)** IL-6 and Cxcl-1 protein concentrations in murine BAL fluid were assessed by ELISA (D) means ± SEM; $n = 5$ mice in the control groups and $n = 9$ mice in the acute lung injury VILI groups; (E) means ± SEM; $n = 4$ mice in the control groups and $n = 9$ or 10 mice in the mimic-223- or mimic-control–treated VILI groups]. **(F)** Representative slides of mouse pulmonary histology before and after treatment with nanoparticles containing *miR-223* mimic (mimic-223) or control mimic (H&E staining). Scale bar, 100 μm. **(G)** Scoring of lung injury in histological sections in (F). **(H** to **J)** Pulmonary transcripts were assessed by real-time RT-PCR relative to the housekeeping gene β-actin for (H) IL-6, (I) Cxcl1, and (J) Tnfα [means ± SEM; $n = 4$ mice in the mimic-control–treated groups and $n = 5$ mice in the mimic-223–treated groups for (H); $n = 4$ mice in the mimic-control-treated groups and $n = 3$ and 5 mice in the mimic-223–treated groups for (I); $n = 4$ and 5 mice in the mimic-control–treated groups and $n = 3$ and 6 mice in the mimic-223–treated groups for (J)] ($^{*}P < 0.05$ and $^{\S}P < 0.05$ in the post hoc analysis between “mimic-ctr"–treated and “mimic-223”–treated mice after VILI, Student's t test or ANOVA).

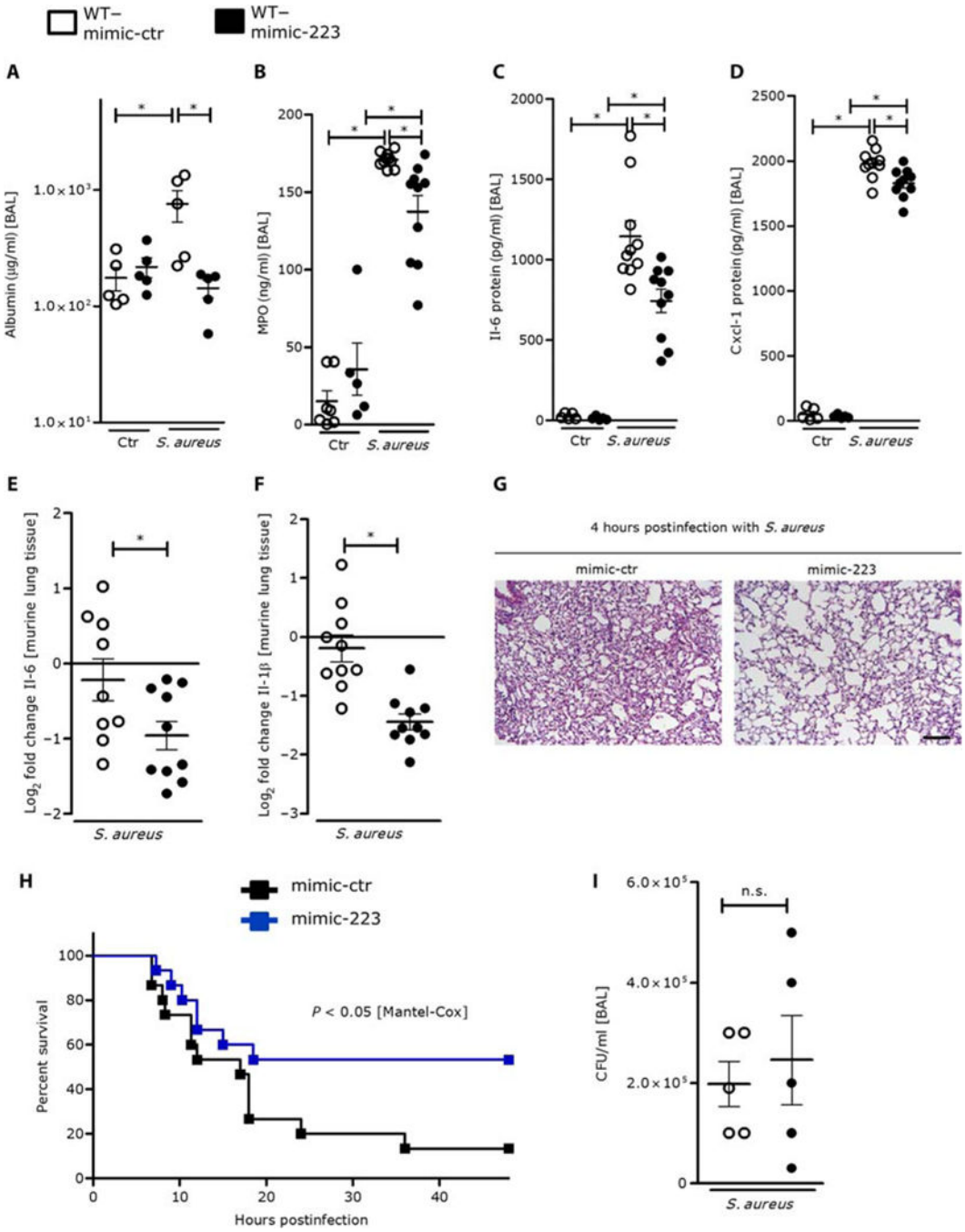

Fig. 8. Pulmonary bacterial infection in C57BL/6J mice overexpressing *miR-223*

After treating C57BL/6J mice with nanoparticles that contained either mimic-223 or mimic-control, mouse lungs were infected with *S. aureus* intratracheally. **(A)** Albumin detected in BAL fluid after *S. aureus* infection and nanoparticle treatment was measured by ELISA (means ± SEM; $n = 5$ mice per group). (**B)** Myeloperoxidase was measured in BAL fluid after *S. aureus* infection and nanoparticle treatment by ELISA (means ± SEM; $n = 7$ and 5 mice in the control groups and $n = 10$ mice in the *S. aureus* infection groups). Protein concentrations of **(C)** IL-6 and **(D)** Cxcl-1 were assessed by ELISA in control and *S.*

aureus–infected C57BL/6J mice [(C and D) means ± SEM; $n = 5$ mice in the control groups and $n = 10$ mice in the *S. aureus* infection groups]. Mouse lung tissue was analyzed for (**E**) IL-6 and **(F)** IL-1β transcripts by real-time RT-PCR relative to the housekeeping gene β-actin [means ± SEM; (E) $n = 9$ mice in the mimic-control–treated group and $n = 10$ mice in the mimic-223-treated group; (F) $n = 10$ mice per group]. **(G)** Representative slides showing pulmonary histology for *S. aureus*–infected WT mice overexpressing *miR-223* (mimic-223) or control mimic (H&E staining). Scale bar, 100 μm (means ± SEM; $n = 5$). **(H)** Mouse survival after pulmonary Infection with *S. aureus* with or without treatment with nanoparticles containing *miR-223* mimic or control mimic ($n = 15$ mice per group). **(I)** Lung bacterial colony-forming units 4 hours after infection of mice with intratracheal *S. aureus* and treated with nanoparticles containing *miR-223* mimic or control mimic (means ± SEM; $n = 5$) (*$P < 0.05$, Student's *t* test ANOVA, or Mantel-Cox test).

Table 1

Characteristics of patients providing BAL fluid samples

hsa-*miR-223* analysis was assessed in BAL fluid collected from 55 patients with ARDS within the first 7 days after diagnosis. Demographic data and APACHE II (Acute Physiology and Chronic Health Evaluation) clinical scores are shown. BAL samples from eight healthy nonsmokers (five males and three females) served as controls, n/a, not applicable.

ARDS patient	Gender	Age	Primary etiology	APACHE II score	ARDS patient	Gender	Age	Primary etiology	APACHE II score
1	Male	27	Aspiration	29	31	Male	63	Sepsis	n/a
2	Male	77	Sepsis	40	32	Female	37	Pneumonia	16
3	Male	37	Pneumonia	n/a	33	Female	37	Sepsis	21
4	Male	37	Pneumonia	15	34	Male	57	Aspiration	21
5	Female	20	Trauma	n/a	35	Male	23	Aspiration	15
6	Female	59	Pancreatitis	33	36	Female	28	Aspiration	18
7	Male	27	Sepsis	n/a	37	Female	57	Aspiration	13
8	Male	62	Sepsis	n/a	38	Male	53	Sepsis	33
9	Female	52	Pneumonia	15	39	Female	42	Sepsis	8
10	Male	48	Sepsis	30	40	Female	50	Aspiration	20
11	Male	59	Sepsis	n/a	41	Male	38	Pneumonia	12
12	Male	37	Pneumonia	15	42	Female	36	Pneumonia	13
13	Female	44	Unknown	21	43	Male	56	Sepsis	18
14	Male	33	Aspiration	13	44	Female	47	Sepsis	9
15	Female	71	Pneumonia	22	45	Male	50	Sepsis	22
16	Male	52	Sepsis	10	46	Female	54	Sepsis	24
17	Female	53	Pneumonia	7	47	Male	58	Pneumonia	23
18	Male	74	Pneumonia	34	48	Male	53	Pancreatitis	19
19	Female	45	Pneumonia	14	49	Male	48	Sepsis	13
20	Female	59	Pancreatitis	20	50	Female	49	Pneumonia	25
21	Male	37	Inhalation	19	51	Male	69	Pancreatitis	19
22	Female	60	Aspiration	14	52	Male	57	Pneumonia	8
23	Male	60	Pneumonia	23	53	Female	43	Aspiration	5
24	Male	64	Aspiration	43	54	Male	50	Pneumonia	24

ARDS patient	Gender	Age	Primary etiology	APACHE II score
25	Male	43	Unknown	22
26	Female	47	Pneumonia	24
27	Male	30	Trauma	20
28	Male	53	Aspiration	27
29	Male	39	Sepsis	13
30	Male	45	Aspiration	30

ARDS patient	Gender	Age	Primary etiology	APACHE II score
55	Male	42	Aspiration	15